A Study and Improvement for Copper Electroforming on Additively Manufactured Mandrels

Zhaohan Zheng

A Thesis

in

The Department

of

Mechanical, Industrial and Aerospace Engineering

Presented in Partial Fulfillment of the Requirements
for the Degree of Master of Applied Science (Mechanical Engineering) at
Concordia University
Montreal, Quebec, Canada

October 2021

CONCORDIA UNIVERSITY

School of Graduate Studies

This is to certify that the thesis prepared

By: Zhaohan Zheng

Entitled: A Study and Improvement for Copper Electroforming on Additively
Manufactured Mandrels

and submitted in partial fulfillment of the requirements for the degree of

Master of Applied Science (Mechanical Engineering)

complies with the regulations of the University and meets the accepted standards with respect to

originality and quality.

Signed by the final Examining Committee:

_____ Chair

Dr. *Carole El Ayoubi*

_____ Examiner

Dr. *Alex De Visscher*

_____ Examiner

Dr. *Carole El Ayoubi*

_____ Supervisor

Dr. *Rolf Wuthrich*

Approved by _____

Dr. *Martin Pugh*   Chair of Department or Graduate Program Director

_____2021   _____

Dr. *Mourad Debbabi*   Dean of Faculty

ABSTRACT

A Study and Improvement for Copper Electroforming on Additively Manufactured Mandrels

Zhaohan Zheng

An idea of combining Additive Manufacturing (AM) and electroforming is coming up for metal manufacturing, which could not only fulfill the increasing needs of low batch size production but also be able to fabricate complex structures like thin-walled components. Compared to direct metal printing, it is more cost-efficient and requests lower energy consumption. However, electroforming on AM mandrel has its limitation in several perspectives. During the process, undesired voids could be build-up, resulting in a rough surface and reduced mechanical properties. Also, the various distance between the mandrel and counter-electrode increased the non-uniformity of the deposit thickness. The outer contour of the deposition is no longer matching the original design.

On the other hand, the thin-walled structures as an essential component in several industrial areas provide several challenges to the conventional manufacturing industry. The difficulty of manufacturing increases along with the aspect ratio. Typically, these structures are fabricated with Electrical Discharge Machining (EDM). With the rise of AM technology, direct metal printing has

recently become a new solution for complex metal structures. However, high porosity and high thermal stress limit direct metal printing in many situations.

In this thesis, several methods are proposed to increase the precision of the electroformed part geometrically. As well as propose a method for thin-walled structure manufacturing, which provides another potential solution for the manufacturing industry.

Acknowledgments

Contribution of authors

Chapter 5   Towards electroforming of copper net-shape parts on additively manufactured mandrels

Zhaohan Zheng[1],   Rolf Wüthrich[1,2]

[1]*Department of Mechanical Industrial and Aerospace Engineering, Concordia University, 1455 De Maisonneuve Blvd. W. Montreal, Quebec, Canada H3G 1M8*

[2]*Department of Chemical and Materials Engineering, Concordia University, 1455 De Maisonneuve Blvd. W. Montreal, Quebec, Canada H3G 1M8*

This paper will be submitted in *Journal of The Electrochemical Society: Focus Issue on Women in Electrochemistry*

Z.Z. and R.W. conceived of the presented idea. Z.Z preformed the experiments and data analysis. R.W. supervised the project and revised the manuscript

Table of Contents

List of Figures

List of Tables

1. Introduction

Nowadays, the industry is moving in the direction of a lower production volume of each design. With the increase in demand for customization, personalization, and rapid prototyping, the batch size for the production becomes much lower and sometimes even requires one. At the same time, the industry-standard, as well as the product quality, need to be maintained at the same or an even higher level. There is no doubt that with the conventional manufacturing method, the production cost for each unit is dramatically lowered by the huge production quantity. While it comes to the low batch size production, the total cost of the conventional mass production process remains at the same level, but the cost for each of the production units becomes unaffordable for most of the customers and the companies.

Additive manufacturing as old technology is well developed recently as the rise of other technologies. Now AM is widely performed as a promising solution for the low batch size production and the personalization for both industrial applications and personal projects. The short design to production time, high manufacturing freedom, and ease of operation make AM a preferred manufacturing process in many cases. The development of modern technologies brings new possibilities to this old technique. AM starts to take a great advantage in manufacturing the complex shape, high accuracy customization, and multi-material fabrication. Since the layer-by-layer fabrication fashion, the non-metal AM process requires no post-processing except the

1

removal of the support structures. Therefore, the complex workflow design in the conventional manufacturing processes is not required for the AM process. The low amount of wastes and the ease of design change and revision make it the most popular fabrication method in rapid prototyping.

However, the limitations of AM are also obvious in many different aspects. The layer-by-layer fabrication nature benefit AM for complex structures manufacturing, but it also brings drawbacks to this method. Since both the inner and outer surfaces are covered with the horizontal line patterns, even the layers are bonded together, AM manufactured structures can be easily delaminated under particular stress in a specific direction. The outer surfaces of the AM fabricated parts except for the bottom that contact the heating plate are also line patterned, which cannot be considered qualified in high precision production. As well, the range of the raw materials available for choose choice is very limited by now, especially for metal production, due to the requirement of thermal properties. AM fabricated parts have a dimension that is highly restricted by the size of the printing chambers. Any over-dimensioned structure needs to be designed separately into several components. Which as well increased the complexity of the process. When it comes to the metal manufacturing process, AM fabricated metal parts always require a dramatic amount of post-processing to reach desired mechanical properties and a fine surface finish. At the same time, the accuracy of the outer surface goes away because of the post-process. Therefore, using AM for those structures which require high accuracy and high standard mechanical properties is not an ideal manufacturing approach.

In the area of metal component production, electroforming becomes a better choice for those structures that specifically require precision. Electroforming, by sharing the same concept with electroplating, is also an application of the electrodeposition process. However, unlike

2

electroplating that only generates a thin coating around the model for different purposes, electroforming generally creates a thick metal deposition that is able to detach from the mandrel or the model and becomes an autonomous part. As the electrodeposition process is an atomic process, a micrometer level tolerance can be reached with proper control of the entire process. The production size is limited mainly by the size of the electrochemical cell, which can be easily adjusted before the process.

However, electroformed layers can be deposited uniformly and precisely under rigorous conditions: a cylindrical-shaped mandrel placed concentrically in a cylindrical-shaped counter-electrode. Changing any of the conditions could result in a non-uniform distribution due to the non-equivalence of the geometrical distance. More important, due to the characteristic of the electroforming process, the formable structures are limited into the extrusion structures, or can also be called two-dimensional structures. Here it brings the design that combines the AM and electroforming. AM provides the design freedom of the structures, and electroforming offers the precision and extra strength of the structures.

This study investigates the non-uniform deposition phenomena on the outer surface of the electroformed parts. Instead of controlling the process with some complex method to achieve a perfect uniformness, an idea of reshaping the mandrel is proposed. Therefore, even with the non-uniform deposition, the outer contour of the electroformed part can be preserved as the original design. Generally, the precision of the outer surface is more critical in most industrial applications. In this case, mandrel modification provides an option that can be simply implemented without changing the other components of the electrochemical cell.

Also, based on the nature of the process, electroforming can be applied to fabricate some specific complex structures like high aspect ratio thin-walled structures. With the conventional

3

subtractive manufacturing process, it is an exceedingly complex process to create thin-walled structures because of the limitation of the cutting tool. At the same time, the electroforming on an AM mandrel can form a structure without the restriction of the dimension. In this study, an idea of the process that enables a multi-level thickness deposit is generated. This idea possibly allows electroforming to become a preferred manufacturing method in more engineering and industrial applications.

2. Literature Review

Additive Manufacturing (AM) is an automated manufacturing technique for fabricating three-dimensional (3D) structures generated by computer-aided designs (CAD) without the need for process planning [1]. The direct and straightforward manufacturing method allows AM to become a competitive method among all different manufacturing processes, especially in the field of rapid prototyping (RP) and customization.

One of the limitations of the AM process is the narrow range of material used for printing. This is evident when it comes to metal printing; the variety of the material is limited, but a significant amount of post-processing is also required to reach the desired dimensional accuracy and mechanical properties.

Electroforming is a process of electrodeposition, and it can deposit metal accurately following the external shape of the mandrel, a mask, or pattern of the design. It also takes advantage of a small amount or no post-process required after the deposition as the smoother surface finish than direct metal 3D printing. Hence, electroforming on a 3D-printed mandrel becomes a promising solution for metal manufacturing. However, many factors can affect the forming result, as it is possible to build up unwanted voids during the process, which could result in an uneven surface with lowered mechanical properties.

In this study, several methods are proposed to improve the geometric accuracy of the electroforming on an AM fabricated mandrel. The result shows that the electroforming process

can be precisely controlled by applying appropriate potential, rotation, and adjustment of the mandrel.

2.1 Electrodeposition

Electrodeposition is a process that deposits metal on conducting surfaces by electric current from a solution that contains ionic species. It is a practical application of electrochemical processes and phenomena[2]. When dissolved in water, acids, base, and salts dissociate into ions. Substances that exhibit dissociation in solution are called electrolytes[2][3]. Ions with a positive charge are called cations; those with a negative charge are called anions. Ions move in an electric field due to their charge cations moving towards the cathode, anions towards the anode. Oxidation/reduction reactions are running the reaction in the electrochemical cells. The cathode gains irons and is in a reduction process, while the anode loses the irons and is in an oxidation process. A general form of the equation for the electrode reactions can be written as:

$$\sum_{ox} v_j X_j + ne^- \rightleftharpoons \sum_{red} v_j X_j \qquad\qquad \text{Eq. 2.1}$$
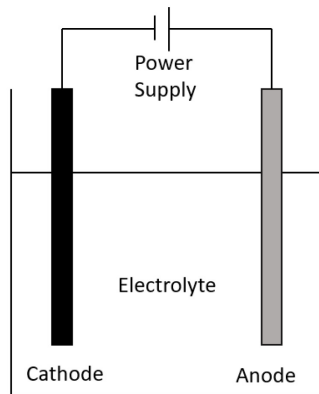
Figure 2.1. Two electrode cell schematics

6

As an atomic process in the conventional industry, electroplating is commonly used for coating, which provides extra mechanical properties for the structures. With the same operation theory, electroforming is considered as the electroplating with a much thicker deposit as well the mandrel will be removed after the process. The deposit itself is considered as an individual part. Recently, more components in the industry that requires high accuracy use electroforming process.

However, only two-dimensional structures can be fabricated with electroforming because of the nature of the process. Only extrusion of the particular pattern can be fabricated with the electroforming.

2.1.1 Faraday's Laws

Faraday's laws, also known as Faraday's laws of electrolysis, are formulated by Michael Faraday. The first law states that the quantities of substances involved in the chemical change at an electrode are proportional to the amount of electric charge Q passed through an electrochemical cell. The second law states: under a given amount of electricity, the mass of different substances released is proportional to their chemical equivalent. The constant, which corresponds to the conversion of one chemical equivalent of substance, called the Faraday constant, has an approximate value of 96485 C mol^{-1} [4]. Therefore, the following equations could be derived, where m is the mass of electrolysis production, an amount of charge Q has been consumed in the cell, the molar mass of the M, and the valence v of the substance deposited at the electrodes. F stands for Faraday constant.

$$m = \frac{Q\,M}{F\,v}$$

Eq. 2.2

For steady currents, Faraday's laws are accurate for charge measuring corresponding to the mass of the substance reacting. During the experiment, it helps control the amount of substance deposited on the electrode through the proper control of applied charge.

2.1.2 Nernst Equation

Nernst equation is an expression that describes the potential change due to the environment change to a nonstandard condition. In an ideal system, with the reaction, the equation could write in a general form:

$$E = E_c^0 = \frac{RT}{z_+F} ln c_{M^{z+}} \qquad\qquad \text{Eq. 2.3}$$

Where R stands for ideal gas constant, F stands for Faraday's constant. At temperature T, with the activity substance c and the corresponding stoichiometric number of the substance c, the potential of the cell can be calculated.

2.1.3 Acid Copper Electrodeposition

As the most common material for electrodeposition, electroplated copper is playing an essential role in a lot of areas, such as conductivity improvement and surface refining [4]. The high plating efficiency and the nature of high conductivity make copper is an excellent choice for an underplate material. In the industry, several methods could be chosen for copper electrodeposition. As one of the earliest electrodeposition methods, acid copper deposition is right now commonly used in the field of electroplating, electrorefining, and electroforming.

Table 2.1. Common Acid Copper Solutions[4]

Copper Sulfate Solutions	Conventional Solutions	High-Throw Solutions
Copper sulfate $CuSO_4 \cdot 5H_2O$, g/L	200-250	60-100
Sulfuric acid H_2SO_4, g/L	45-90	180-270
Chloride, mg/L	—	50-100
Copper Fluoborate	Low-Concentration Solutions	High-Concentration Solutions
Copper fluoborate, $Cu(BF_4)_2$, g/L	225	450
Fluoboric acid, HBF_4, g/L	15	30
Boric acid, H_3BO_3, g/L	15	30

The sulfate, chloride, and fluoborite salt are common choices for the electrolyte. The high conductivity of the solution and small electrode polarization allow lower voltage requirements for the acid copper solution than the alkaline solution. When applying low current densities inefficiently agitated, purified solution, anode and cathode polarizations are nearly negligible. The electrode polarization may occur when exceeding a current density of 5 A dm^{-2} on the anode. Some additional agents are necessary to improve the quality of the deposit. For example, organic compounds and surfactants are common additives for a smoother and brighter surface finish. [4][5].

Another operating condition may also be required on the requirement of the deposit result. The conditions include and are not limited to temperature control, current density control, electrolyte agitation, and electrolyte filtration and purification[4].

2.1.4 Mass Transfer in the Electrochemical Cell

Electrolyte migration, diffusion, and convection, which are the three categories of mass transport, retain the mass balance in the cell [2]. Migration is the movement of charged particles according to an electric field. Figure 1.2 shows the process of migration.
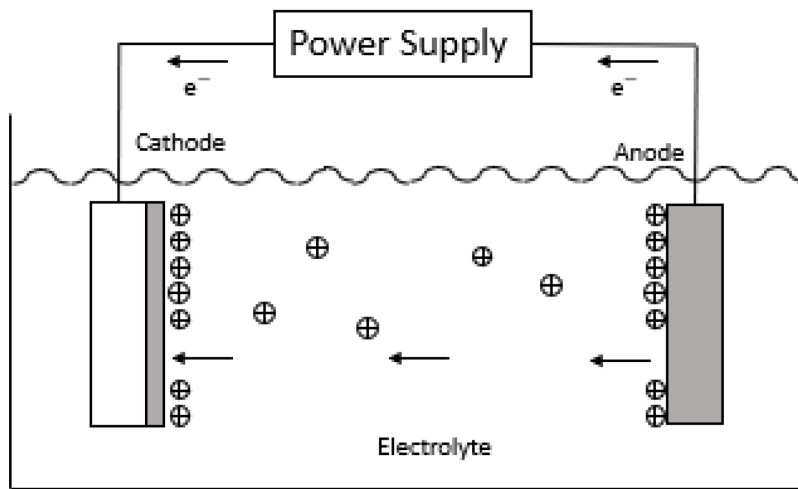
Figure 2.2. Migration of metal ions from a anode to the cathode [6].

The random movement caused by the concentration difference of the molecules is called diffusion. Particles diffuse from a more concentrated region to a less focused area with a coefficient determined by the nature of particles. Without any forced convention, the thickness of the diffuse layer is also known as the Nernst layer, has an approximate layer thickness of 0.2mm.
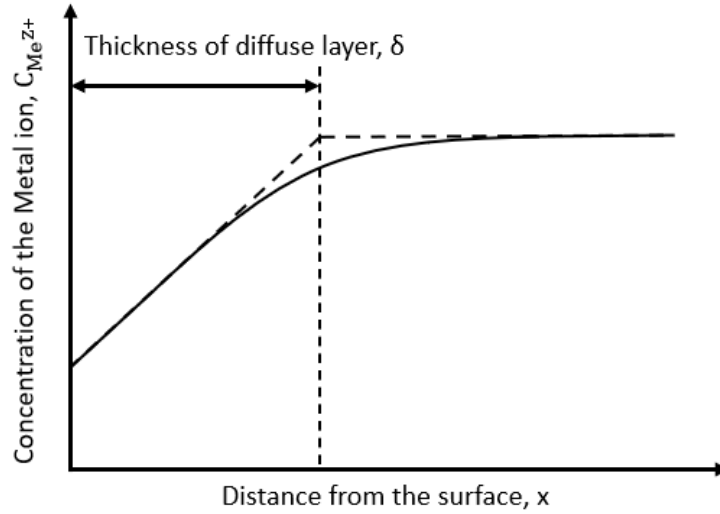
Figure 2.3 Metal ion concentration profile as a function of distance from the surface[6].

According to Fick's first law, a linear relationship exists between the diffusion flux and the decrease of a concentration gradient in the direction of decreasing concentrations. The equation is generally written like this:

$$J_{d,j} = -D_j \, grad \, c_j \qquad \text{Eq. 2.4}$$

Where $J_{d,j}$ is the diffusion flux, and D_j is the diffusion coefficient of the particles [2][7].

Under the simultaneous effects, the total ionic flux by migration and diffusion of an electrostatic field E can be written in Nernst-Planck equation like:

$$J_j = J_{m,j} - J_{d,j} = c_j u_j E - D_j \frac{dc_j}{dx} \qquad \text{Eq. 2.5}$$

11

Convection is a bulk movement of the particles when the electrolyte has an involuntary action. It is usually the natural convention or agitation from external mechanical structures [8]. During the electrodeposition process, there is a theoretical maximum current flow through the cell called limiting current. With natural convection, the effect of migration can be eliminated limiting current is determined by diffusion[9]. While an appropriate agitation is applied, a laminar flow pass through the surface of the electrode. Mass transport becomes conventional limited.

2.1.5 Reference Electrode

To control the potential of the working electrode and take the measurements, the reference electrode is introduced into the cell [10]. It is the reference electrode that allows the investigation of the particular electrode potential. One of the characteristics of the reference electrode is non-polarizable theoretically. In many simple cases where thermodynamic equilibrium does not exist, the pseudo-reference electrode is used instead of a proper reference electrode. It only requires direct immersion in the solution. The pseudo-reference's main advantages are the simplicity of use, low ohmic resistance, and zero contamination to the solution. Meanwhile, the lack of the thermodynamic equilibrium, the possibility of polarization, and limited work conditions such as pH and temperature are the main drawback of the pseudo-reference electrode[11].

2.1.6 Pulse Reverse Electroplating

In pulse electrodeposition (PED), the electric potential or current alternates rapidly between two different values. This results in a series of pulses of the same amplitude, either with a same

duration or same amount of charge as well as the polarity. As shown in Figure 2.4, each pulse includes an application time and current on-time (TON) and a zero current on-time (TOFF).
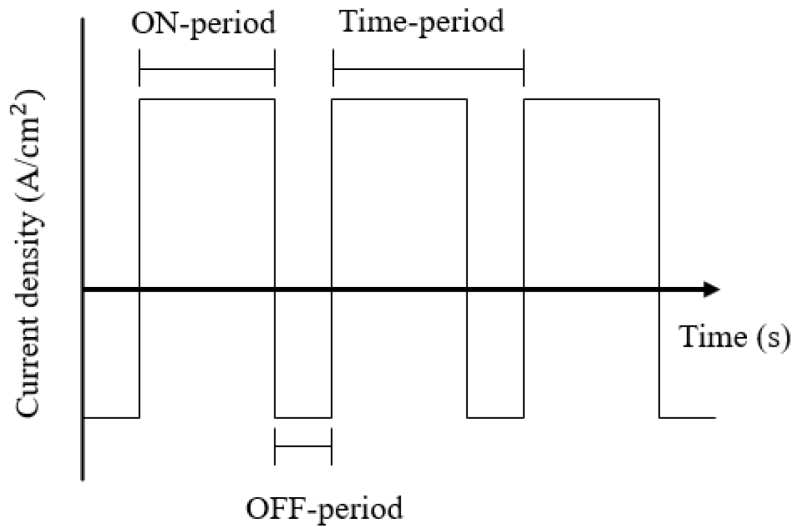
Figure 2.4. Typical pulse-current waveform[4]

The composition and thickness of the deposited film in atomic order can be controlled by adjusting the pulse amplitude and width. They are conducive to the formation of grain nuclei and significantly increase the number of grains per unit area, resulting in fine-grain deposits with better performance than conventional coatings.

The peak current, peak potential, frequency, and duty cycle are the usual experimental parameters. The maximum setting of the current electroplating is called peak current. The duty cycle is the practical portion of time during which a current or potential is applied in a particular plating cycle. The effective current/potential is obtained by multiplying the duty cycle or the

13

present or potential peak value. Pulse electroplating can help improve the quality of the electroplated film and release the internal stress accumulated during the rapid deposition process. A high frequency with a short plating duration can dramatically reduce the surface roughness. With the same duty cycle and frequency, a higher peak potential can also result in a rough surface. The electroplated material has a potential risk of contamination because of the reverse plating process (the electropolishing process). Therefore, the application of the pulse reverse plating process needs to be a well concern for those costly materials.

2.1.7 Uniformity of the Deposition

Non-uniform electrodeposition can cause lower mechanical properties and decrease dimensional accuracy[12][13]. In general, the uniform deposit is caused by the uniform distribution of the current density. On the other hand, the non-uniform current density commonly occurs on the edges and corners, resulting in a non-uniform deposition on these regions. Therefore, the corners and edges usually have more deposits than the other region caused by the "edge effect"[14]. In the industry, many of the methods are proposed in order to avoid the edge effect.

Shields and baffles are traditionally used in the industry to control the geometry of the deposition on a flat surface. A non-conductive structure that is used for directing the current flow is called a shield. The structures are used to intercept the current flow are called baffles. With a properly positioned shield or baffles, a surprising amount of extra deposition on the corners and edges can be eliminated.[15].
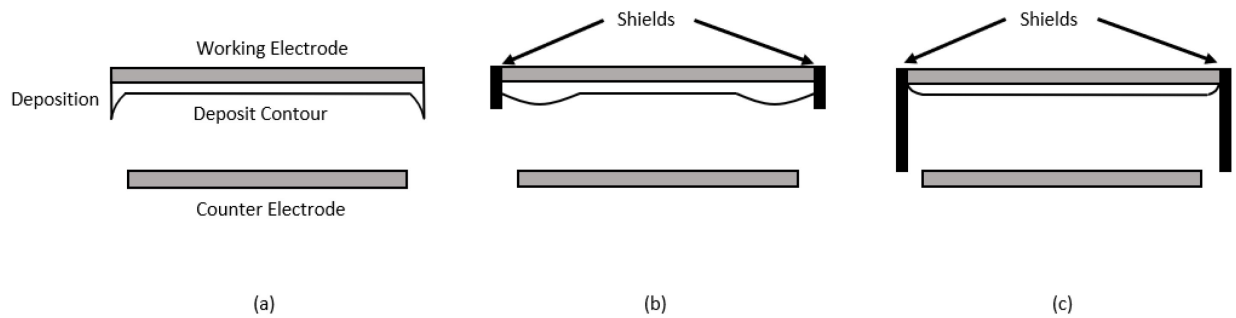
Figure 2.5. Distribution patterns obtained with different shields and the same anode-cathode spacing: (a) poor distribution with no shield; (b) fair distribution obtained with a narrow shield; and (c) good distribution obtained with a wide shield[16].

The use of multi-anode baths is also applied to improve the uniformity of the electrodeposition. According to the geometry of the working electrode, several counter electrodes are placed around it. Each of the anodes needs to be located precisely based on the calculation. This method is more suitable for coating and forming a uniform deposit for a three-dimensional structure. With the multiple anodes around the working electrode, the uniformity of the current density is improved by the well-distributed electric field. While, the disadvantages of the approaches include the extra cost for the extra anodes, additional modeling, and construction workload for precise positioning of each component of the electrochemical bath [14]. As well this method is less applicable for fabricating multiple parts at the same time. On the other hand, it is inefficient for mass production or mass customization.
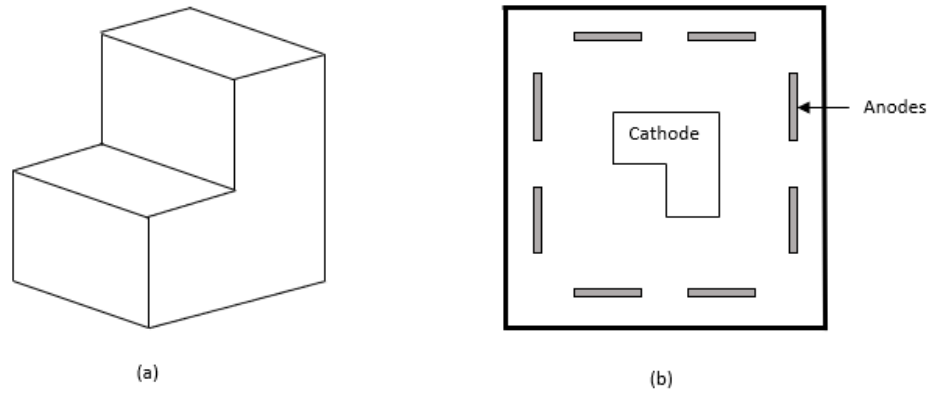
Figure 2.6. Schematic diagram of the multiple anodes electroplating bath. (a) A 3-dimensional isometric view of the cathode. (b) the location of the muti-anodes and cathode placed in the electrochemical cell [14].

By using a similar principle, instead of using multiple anodes, a conformal anode can also remarkably improve the deposit uniformness by improving the uniformness of the current density distribution on the working electrode as well [13]. Same as the muti-anodes method, this method requires extra workload to reshape the anode. The setup with the conformal anode becomes a method specifically for single part electroplating.
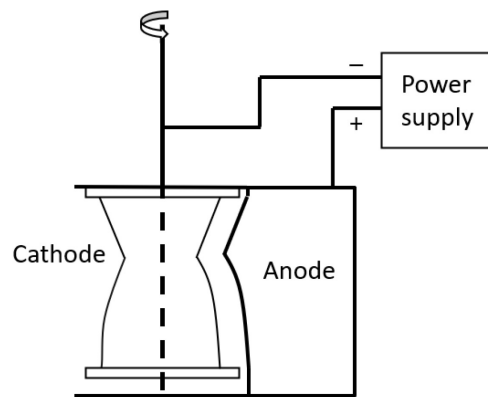
Figure 2.7. Schematic diagram of the electroforming cell for revolving parts [13].

16

Since both of the two methods require the extra modification on the counter-electrode setup to fit different structures of working-electrode, these methods are not appropriate for manufacturing numerous parts simultaneously and require extra cost and labor for any of the changes on the structures.

2.2 Introduction to Additive Manufacturing

Additive Manufacturing (AM) is a layer-wise manufacturing technology that is developing rapidly in recent years [17]. The horizontal layer builds up on top of another rise the vertical dimension to construct a three-dimensional object. As a standard method used in industrial design, rapid prototyping (RP) is one of the most popular applications of AM. The processing time from a three-dimensional Computer-Aided Design generation to a completed part is dramatically shortened with AM. Compared to other manufacturing processes, AM takes advantage of full automation since no extra detailed analysis or planning is required[18].

Presently, AM also has many problems and disadvantages in a lot of aspects. Firstly, the choices of the material are minimal, especially in the metal category. Only a narrow range of the variety can be printed with current technology. Secondly, finishing procedures are required for AM process to get mechanical properties and a surface finishing as good as the traditional manufacturing process. Also, the cycle times are pretty long for repeating part production with no cost reduction compared to the conventional manufacturing method. Therefore, indirect prototyping might apply to improve the AM process. Depending on the requirement, engineers could select proper procedures to fulfill the needs.

2.2.1 Development of Additive Manufacturing Technology

The invention of the computer brings a lot of new technologies, including AM. Not as novel as people might think, AM was used commercially in the late 1980s. Unlike other well-known AM technologies, SLA (stereolithography apparatus) machine was the first patented machine globally. Later, companies from all over the world started to launch the new system. Early 1990's, fused deposition modeling (FDM), solid ground curing (SGC), laminated object manufacturing (LOM), selective laser sintering (SLS), and direct shell production casting (DSPC) were coming into the market successively[19]. With the spreading of the desktop, FDM 3D printers lead by the makers' community and breakthroughs in the medical application in the early 2000's make AM a popular topic. Many different ideas came up after. Presently, the AM process is now moving towards precision manufacturing and microstructure manufacturing [20]. As well, the increasing variety of the materials join the AM family, more printable materials are available commercially. A tabletop FDM printer is now standard equipment for many laboratories and institutes. For many three-dimensional complex structures, AM remarkably simplifies the process of production[1].

2.2.2 Fused Deposition Modeling Printer

AM technologies contain extensive methods for fabrication. Therefore, classification becomes a non-negligible issue for this subject. A two-dimensional classification method was introduced by D.T Pham based on the single-layer construction method and the type of raw material input[21].
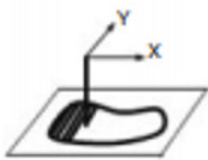
	1D Channel	2x1D Channels	Array of 1D Channels	2D Channel
Liquid Polymer	SLA (3D Sys)	Dual beam SLA (3D Sys)	Objet	Envisiontech MicroTEC
Discrete Particles	SLS (3D Sys), LST (EOS), LENS Phenix, SDM	LST (EOS)	3D Printing	DPS
Molten Mat.	FDM, Solidscape		ThermoJet	
Solid sheets	Solido PLT (KIRA)			

Figure 2.8. AM classification by Pham (the diagram has been amended to include recent AM technologies) [1]

Other classification methods exist as well. One of them is based on the type of processing (Table 2.2). The process-based classification is more beneficial for the AM technology selection depending on the usage and material of the structure. Each of the processes has its advantages in certain aspects as well the imperfection in the other aspects. In order to select an appropriate process and balance through different properties of the final product, the decision needs to be made with extra carefulness.

19

Table 2.2. AM classification based on the type of the process [22]

AM Process Group	Typical Commercial Names	Related Material Type
Vat Photopolymerization	Stereolithography (SLS) Digital Light Process (DLP) Solid Ground Curing (SGC) Projection Stereolithography (PSL)	Polymers Ceramics and wax
Powder Bed Fusion	Electron Beam Melting (EBM) Electron Beam Additive Manufacturing Selective Laser Sintering (SLS) Selective Heat Sintering (SHS) Direct Metal Laser Sintering (DMLS) Selective Laser Melting (SLM) Laser Beam Melting (LBM)	Polymers Metals Ceramics, sand, and carbon
Directed Energy Deposition	Laser Metal Deposition (LMD) Direct Metal Deposition (DMD) Direct Laser Deposition (DLD) Laser Engineered Net Shaping (LENS) Electron-Beam Freeform Fabrication (EBFF) Weld-based Additive Manufacturing (WAM)	Powder Metals
Binder Jetting	Powder Bed and Inkjet Head (PBIH) Plaster-based 3D Printing (PP)	Polymers Metals Glass
Material Extrusion	Fused Deposition Modelling (FDM) Fused Filament Fabrication (FFF)	Polymers Sand
Material Jetting	Multi-Jet Modelling (MJM)	Polymers Metals Wax and biomaterial
Sheet Lamination	Laminated Object Manufacturing (LOM) Ultrasonic Consolidation (UC)	Polymers Metals

Among all the different AM processes, fused deposition modeling FDM is emphasized in the project. By feeding the thermoplastic filament into a heated extrusion head, melted viscous polymer can be extruded out of the nozzle tip. A two-dimensional motion controlled by a computer form one layer. The Z-axis motion allows the "layers" to stack up on top of each other to create a three-dimensional structure, as shown in Figure 2.9.
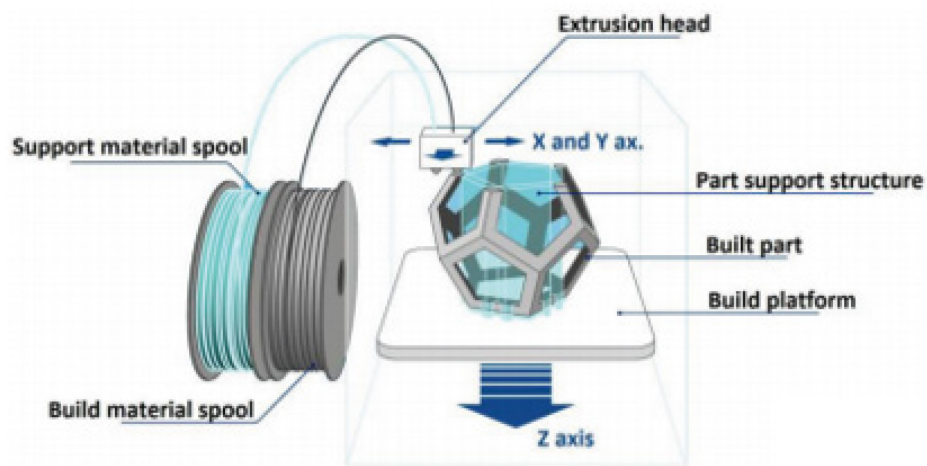
Figure 2.9. Conceptual sketch of FDM [23]

Polylactic acid (PLA) and acrylonitrile butadiene styrene (ABS) are the most common filament used for FDM printers. A generic fabrication process always starts with computer-aided design (CAD) modeling, a solid need to be created for further operation. The completed CAD model needs to be converted into STL format; a universal format taken by slicing software. STL format contains only the information of the external surface required for slicing. An FDM printer either comes with its slicer or has a set of parameters to work with another open-source slicer. These slicers have adjustable parameters and generate the G-code, a numerical control programming

language, based on the requirements. After transferring the corresponding G-code to the machine, the printer is ready to extrude the object. Post processes are negligible for FDM machines. Usually, only brims and support structures need to be removed before being prepared to be used.

2.2.3 Metal Additive Manufacturing and Post-Processing

Similar to other AM technologies, direct metal AM processes are existing since the last century. However, as several critical improvements have been developed in the '20s, the natural metal process, also known as direct metal printing, becomes applicable and visible in the industry field[1]. Usually, metal AM methods are classified into two groups: powder bed system and powder feed system.
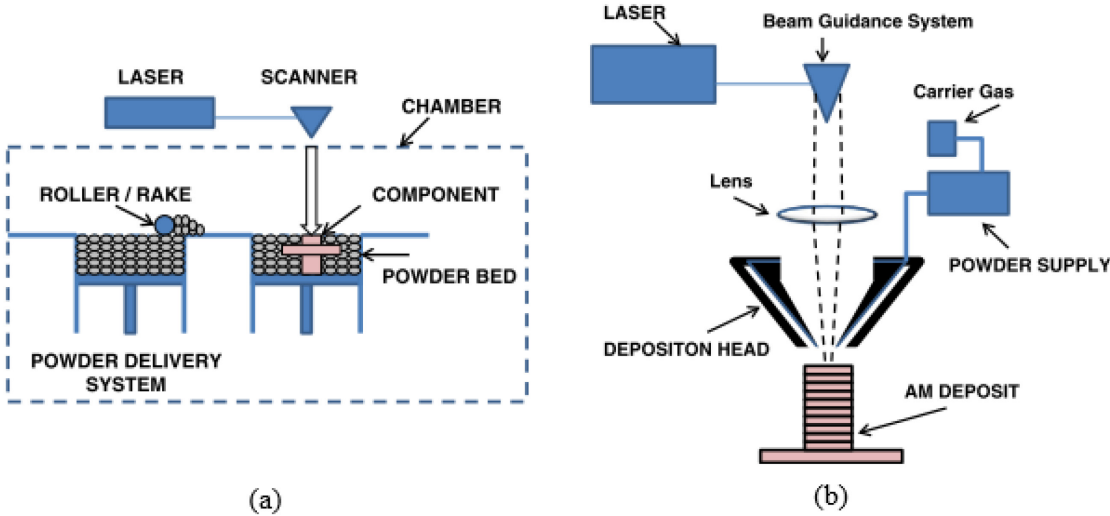
Figure 2.10. Schematic diagram of the AM powder system: (a) Generic illustration of an AM powder bed system. (b) Detailed illustration of the AM powder feeding system [24].

2.2.4 Opportunities and Future Directions

In recent days, the demands of mass personalization and customization production are increasing rapidly [25]. The spreading of lean manufacturing thesis drives the factory from mass production to just-in-time (JIT) production [26]. For both cases above, low batch size production is required for higher cost-efficiency and work efficiency [27]. With the conventional manufacturing method, expected batch size production usually comes more costly, especially for parts with increased complexity. The nature of AM makes it a competitive process for low batch size production, as shown in Fig.1.8., concerning injection molding, the lower production quantities, the higher cost-efficiency AM has. The increasing complexity of the parts even enlarges the difference.
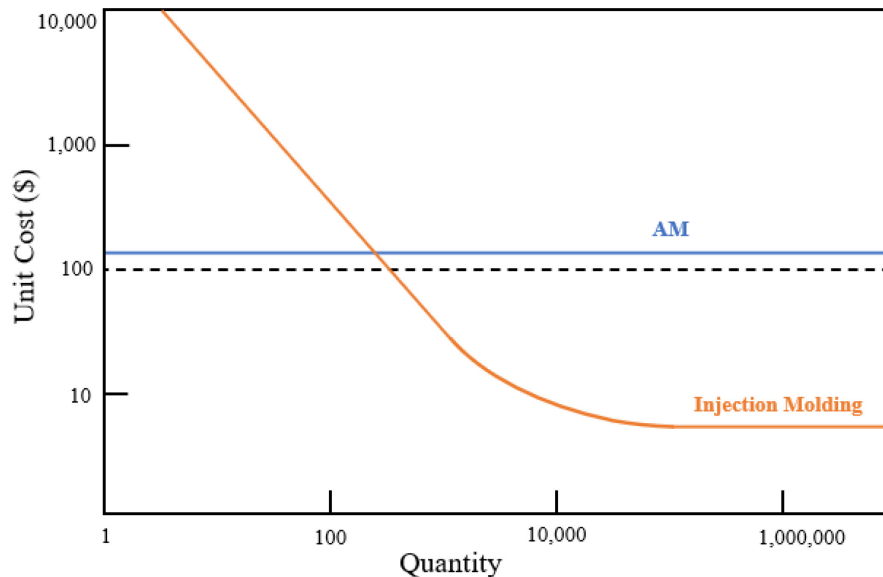
Figure 2.11. The cost for production of 1kg polyamide part as a function of the number of identical parts and the cost per piece. The shift of the injection molding to the right is associated with an increase in geometric complexity of the part [28].

However, AM process comes with several significant issues before introducing in further application. The AM systems and related materials which could satisfy the industry standards are high-priced. Some of the material, for example, metal, requires an extensive amount of manual post-processing before acceptance for use. Common post-processes include support structure removal, heat treatment, sanding, polishing, coating, etc.[17][29]. A vision of a fully automated AM process can be seen in the future. The entire system will no longer require manual effort and can have a ready-to-use output part. AM production can extend its capability by integrating with other manufacturing technologies. Although AM cannot substitute conventional manufacturing in many industries, it provides plenty of possibilities for fresh ideas and novel technologies[30].

2.3 Thin-walled Structures

A thin-walled structure is a general structure group that is hard to define quantitatively. Compared to other cross-sectional dimensions of the part, one or more portions of the structure with a much smaller thickness can be considered as a thin-walled structure. In many engineering applications, thin-walled structures are acting a significant role [31]. In the application of automobile, the lightweight and excellent energy absorption capability makes these structures qualify to protect the occupants from the impact energy [32]. To balance between the technical properties and its economical operation, the modern aircraft, especially the load-bearing structures, are exclusively constructed with thin-walled structures, which could as well minimize the structural mass [33]. The high flexibility of the thin-walled structures made them easier to shape into different cross-sections. As well because of the high flexibility, the complexity of the structure and its behavior is also increased.

2.3.1 High Aspect Ratio Structure

Aspect ratio describes the ratio of an object's width to height[34]. Thin-walled high-aspect-ratio structure manufacturing gain lots of attention as the usage for lightweight components. Especially in the area of aeronautical and aerospace engineering. In the field of manufacturing, these parts are pretty challenging for conventional subtractive manufacturing methods [31].

Recently, electrical discharge machining (EDM) has been used to manufacture complex structures with high precision on any conductive material. However, the poor surface quality, residual stress, and slowness during the process make EDM only applicable in limited condition [35]. On the other hand, with the spread of additive manufacturing, the laser powder bed fusion process (LPBF) is now used for customized thin-wall structures. The minimum wall thickness and the dimensional accuracy are limited by the specifications of the machine and the powder size of the raw material [36].

3. Objective

Electroforming is another potential solution for low batch size metal production. As an electroformed part can theoretically reach atomic precision with a better mechanical property, it could be a better selection in many applications compared to AM process. Therefore, this study is presented to address the issue of electroforming on an AM manufactured mandrel for further improvement.

In this thesis, two major targets are established. Firstly, the problem of the non-uniform deposit is addressed. The non-uniformness is caused by the varied distance between the mandrel surface and counter-electrode. Several researchers tried to figure out an approach that can force the deposit to form uniformly. However, instead of having a uniform deposit, a desired net shape of the deposit is more essential for the application. This study focuses on discovering the regular pattern of the electrodeposition variation and proposes a method that modifies the mandrel to reach the desired net shape.

The second target of this study is proposing a new mandrel design. In the actual manufacturing industry, a uniformly plated part cannot satisfy all the possible situations. Therefore, a mandrel that enables a multi-thickness deposit can further broaden the application of the electroforming process.

4. Experimental Procedure

4.1 Mandrel design

Various designs of the mandrel are created by using Computer-Aided Design (CAD) software. The CAD model needs to be exported in the STL format: a format only stores geometrical data of the surface of the three-dimensional object. Ultimaker Cura, a slicing software, is used to open the STL formatted file and adjusts parameters during the printing. A 0.25mm diameter nozzle with a layer height of 0.15mm is selected in order to balance the precision and printing speed. Wall thickness as well as the top and bottom thickness are set to 3mm to achieve a rigid shape. Another critical factor is the 5mm brim needed for better adhesion during the printing, avoiding deformation caused by the temperature difference between the hot printing plate and the room temperature. The mandrels are printed by an Ultimaker 2+ Fused Deposition Modeling (FDM) printer using black ABS filaments (flaments.ca). After printing, let the printer cool down by itself till the printing plate has near room temperature. Separate parts from the printing plate and carefully remove the brim.

As the electrolytic copper forming process is selected for the study, a direct electric current needs to pass through the desired surface to enable the deposition. Low conductivity can result in a void build-up and rough deposit on the surface. The conductivity of the mandrel surface and solid connection are vital for this experiment. Selection of mandrel fabrication process below:

Conductive Filament Mandrel

Printing the mandrel with conductive filament is the first method tested. The tested filament is called simple copper filament from filaments.ca. The printed mandrel has a very high electrical resistance for over 100 Ω, while the objective of the resistance is lower than 10Ω. Also, the surface of the printed mandrel has an uneven and non-smooth surface because of the layer-by-layer fabrication nature of the FDM printing.

ABS printed mandrel spayed with conductive paint

Conductive paint can be applied on the mandrel to enable the connection on the surface. ABS is selected as the printing since it can be dissolved in Acetone and separated with the deposit. A conductive copper paint (Caswell) is tested sequentially with a paintbrush and a spray gun. The conductivity is much better than the conductive filament, while the conductivity is not consistent throughout the surface, resulting in numerous voids building up during the electroforming. As well as the coating deteriorates when the mandrel is immersed in the solution.

ABS printed mandrel covered with copper foil

Here comes the final potential solution and the selected solution: apply a thin pure copper foil with glue on one side (3M) on top of the ABS printed mandrel. It provides meager and consistent electrical resistance (0.2 Ω) throughout the covered surface. The thickness of the foil can be negligible since it only has a thickness of 0.066mm and uniform thickness throughout the surface[37]. Another benefit of the copper foil is that the finished surface is clean and smooth

compared to the other two kinds of mandrel. Copper foil can flatten the uneven surface generated during mandrel printing.

<center>(a)   (b)   (c)</center>
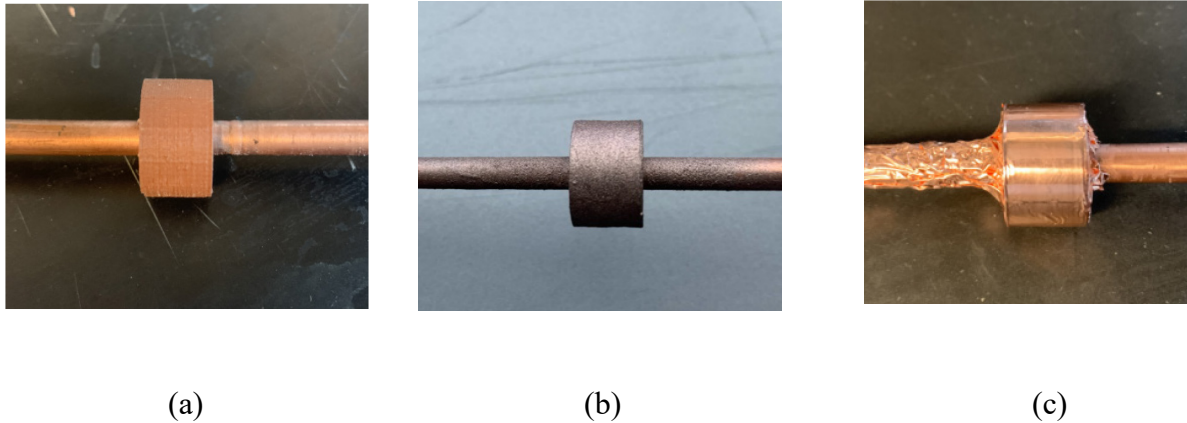
Figure 4.1. Different conductive mandrel fabrication method. (a) Mandrel printed with conductive filaments. (b) Mandrel coated with copper paint. (c) Mandrel covered with copper foil.

4.2 Experiment setup system development

During the experiment, in order to have a controlled rotation of the mandrel, a spindle was controlled to rotate the mandrel during the electroforming process. A self-integrated system controls the rotation, which uses a Raspberry Pi 3B microprocessor as a controller. The stepper motor is powered by an external power source. A motor driver is used to communicate with Raspberry Pi. On the software side, as it shows in appendix A, a pulse-width modulation (PWM) method is utilized to manage the rotational speed and limit the current for long-term operation. In

order to increase the mass transfer around the working electrode, a rotation speed of 200 rpm is applied for the study.

(a) (b)
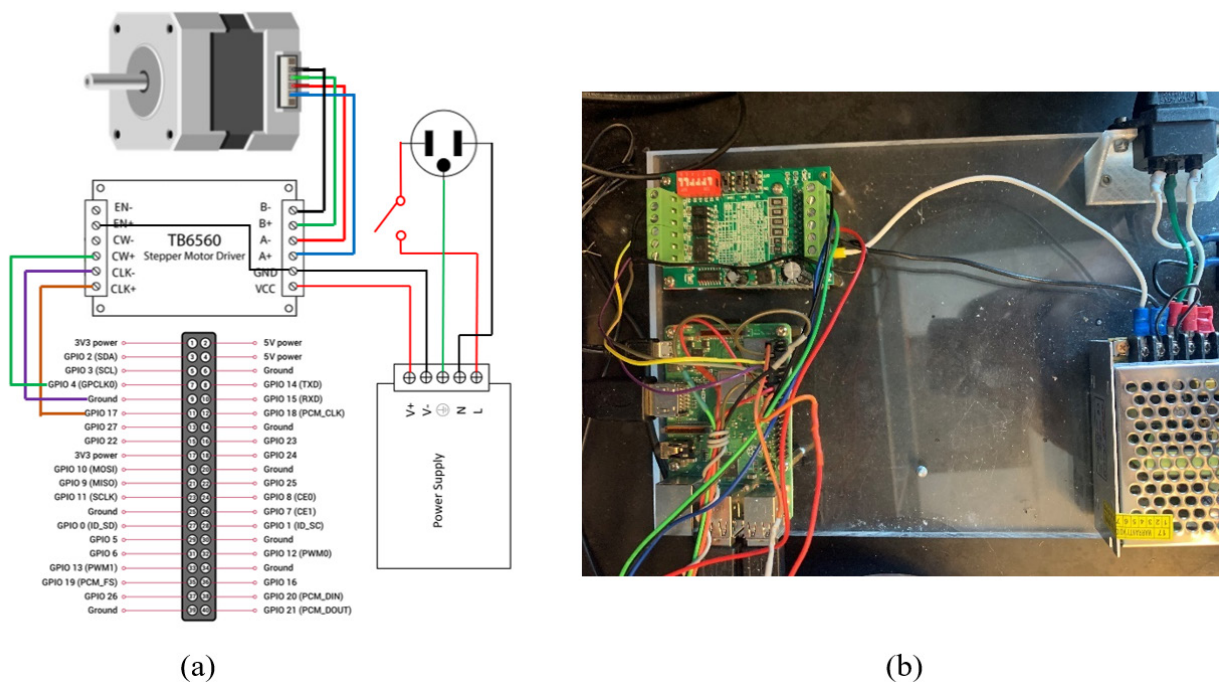
Figure 4.2. Rotational control (a) Circuit drawing (b) The finalized control system of the spindle

4.3 Electrolyte and electrochemical cell preparation

A solution of 1M H_2SO_4 (98.08%, J.T.Baker) and 0.5M $CuSO_4 \cdot 5H_2O$ (98.0%, Sigma-Aldrich) prepared with deionized water is selected as the electrolyte in this study, as it provides both enough amount of y copper(II)-ions and conductivity for the electroforming process (Figure 4.3)[37].
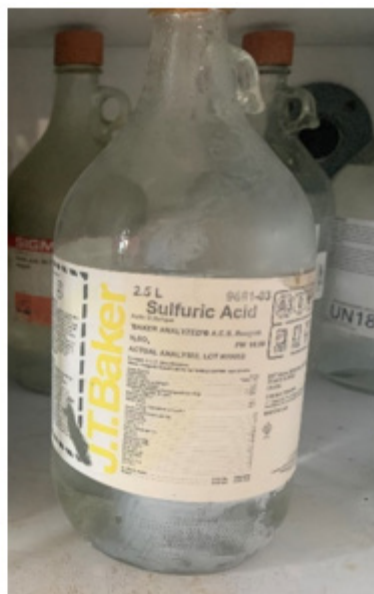
Figure 4.3. Electrolyte preparation (a) Copper(II) sulfate pentahydrate from Sigma-Aldrich. (b) Sulfuric Acid from J.T.Baker

The mandrel fixed on the copper rod is mounted on a spindle. The conductivity is ensured by rolling a stripped electrical wire around the copper rod. The counter electrode is a copper sheet rolled in a cylindrical shape with 9cm diameter and 6cm height. In order to maintain the shape of the counter electrode and fixed to the center of the container, a printed ABS fixture is applied around the counter electrode and connected to the fixture on top of the container. A 1mm diameter copper wire is served as a pseudo-reference electrode located about 5mm away from the working electrode. The entire glass container sits on top of a magnetic stirrer stage for extra agitation through the forming process. The three electrodes are shown in Figure 4.4a, all connected to a Ministat XL (Sycopel Scientific Ltd.), the potentiostat used in the experiment to continuously

provide a steady potential over this three-electrode cell and monitor the current flow through the

working electrode.
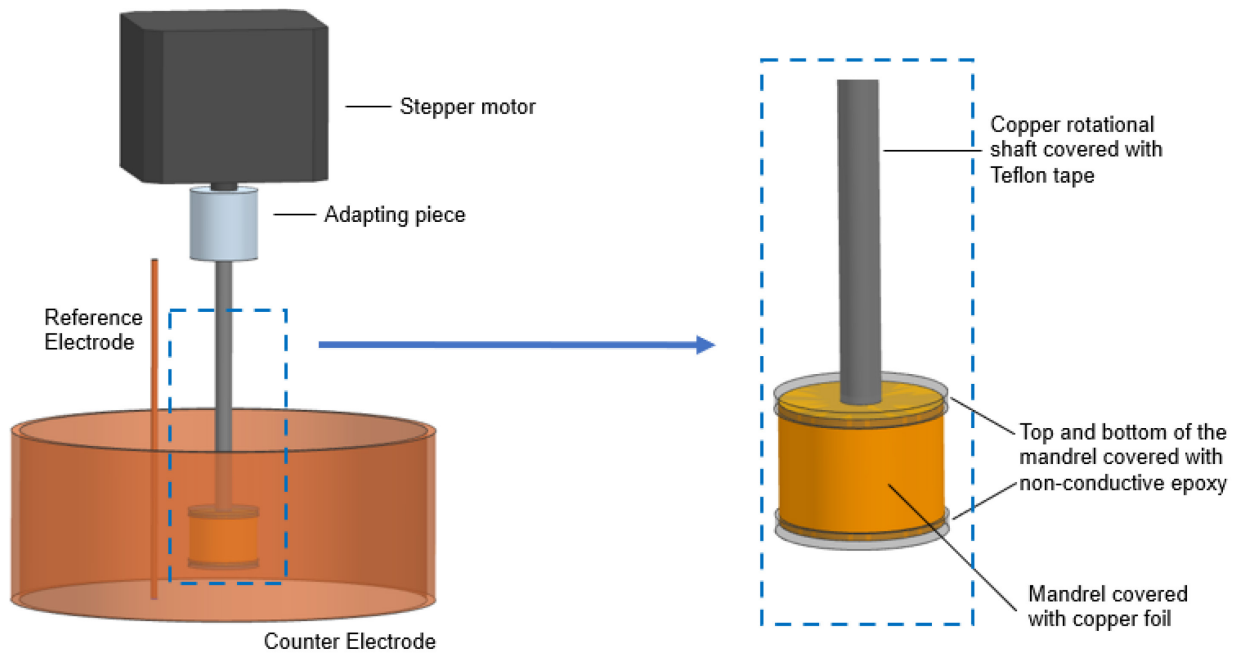
Figure 4.4. A schematic of the electroforming setup. (a) An overview of the electrochemical

cell setup with the connection. (b) A detailed drawing of the mandrel
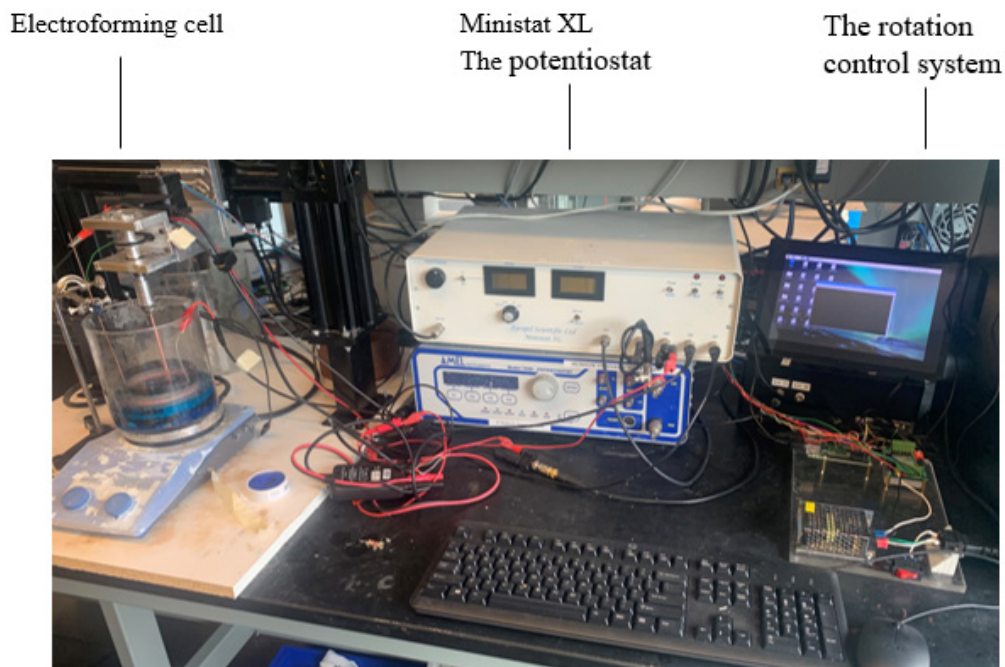
Figure 4.5. The complete electroforming setup

4.4 Electroforming process

In the experiment a three electrodes mode of the potentiostat and an in-house developed system ECTk [38] is able to control the potentiostat to output desired potentiostat. In order to avoid the formation of the cauliflower structures and hydrogen co-depositions, a deposition pulses at -150mV is applied [37]. An +100mV electropolishing pulse removes 10% of the deposition charge to achieve a better surface finish. Because the deposit thickness is directly related to the amount of applied charge, the layer thickness of each pulse can be properly controlled by fixing the amount of deposition charge. Therefore, instead of a fixed time deposition, a fixed charge deposition was made. Each cathodic pulse deposits a charge of 2.7886 C/cm^2. Approximately 1 micrometer of the deposition can be created. Two of the pulses are activated alternately until the desired thickness is

formed on the mandrel. Therefore, the deposition thickness can be manipulated by the number of deposited pluses.
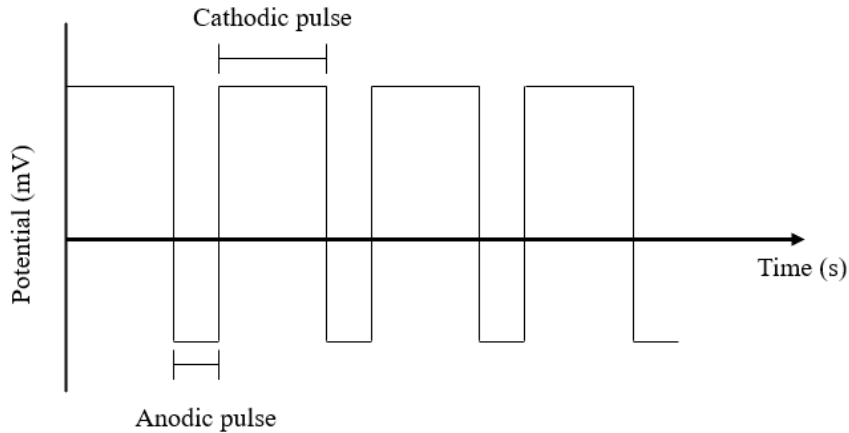
Figure 4.6. Pulse reverse electroforming cycles diagram

4.5 Thickness Determination Procedure

4.5.1 Post Experiment Process

After desired thickness is deposited on the mandrel, the mandrel needs to be removed from the solution, cleaned thoroughly with deionized water, and completely dried with airflow. The improper cleaning procedure will result in the oxidization of the copper in the following procedures. A cold mounting epoxy (MetLab Corporation) and two sizes of the reusable plastic mold (1inch and 1.5 inches in diameter) are used to mount the mandrel.

For the purpose of clearly revealing the cross-section of the mandrel, the solidified cold mounted mandrel will be polished on a MetaServ 250 grinder. A 400-grid sandpaper is applied to remove the top layer of the material until the cross-section of the mandrel is clearly revealed. Then the polishing procedure is repeated with a sandpaper grade of 600, 800, and 1200. Finally, a further polish with 1μm MetaDi Polycrystalline Diamond Suspension polishing paste is applied for a clear surface. The pictures of the mandrel's cross-sections were taken with a VHX-500 microscope with a magnification of 30x.

4.5.2 Image processing

The microscope pictures are processed with a self-developed MATLAB program to avoid color confusion and simplify the programming procedure. The microscope pictures were manually refined first with pure black color (RGB 0,0,0) to eliminate the interferences of different colors (Figure 4.7a).
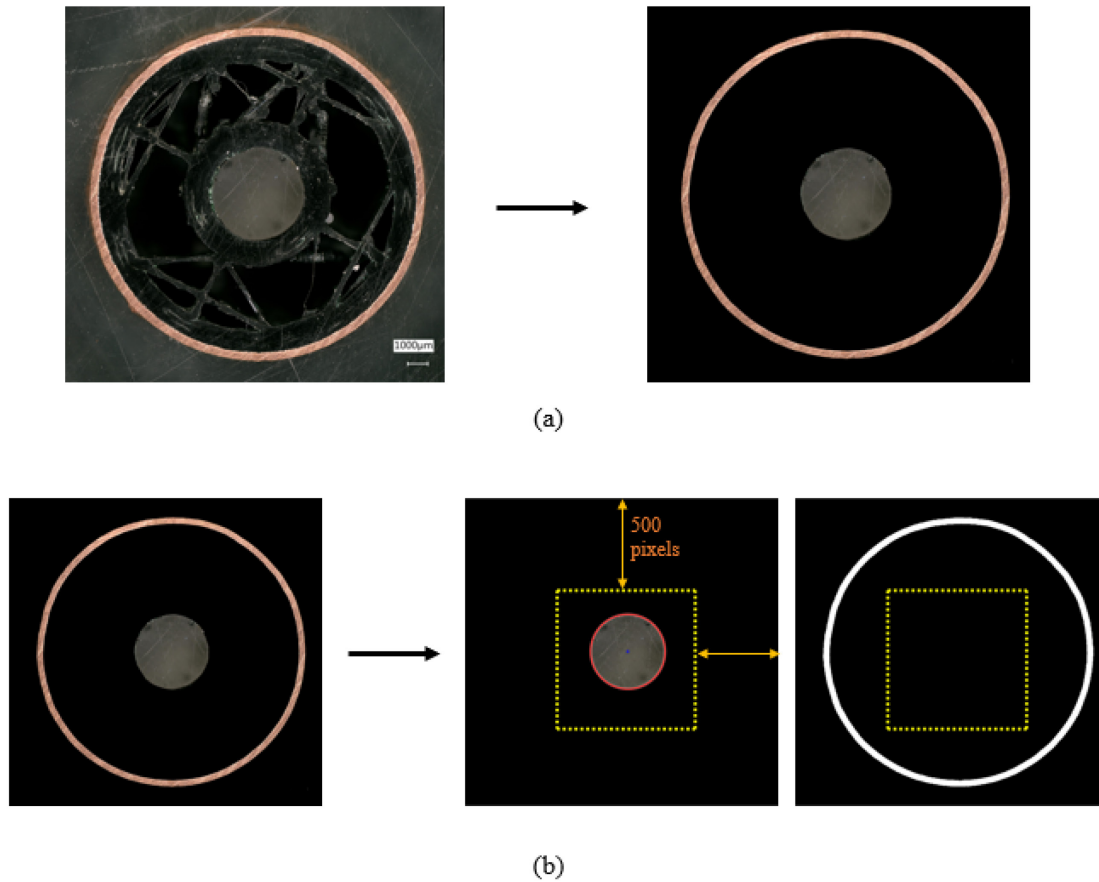
Figure 4.7. Image refining procedures. (a) Color elimination. (b) Image separation.

Then the image needs to be further separated into two parts: one contains the through-hole mounting the rotational shaft, and the other contains the deposit contour. This process was automatically done by a MATLAB function (Appendix B.2) based on their locational difference: the area with a distance of 500 pixels counting from each edge was considered as the area contains the copper deposit, and the area left in the middle was considered as the region of the through-hole (Figure 4.7b). Then the image that contains the through-hole was additionally operated with a build-in MATLAB function 'regionprops', which can obtain several properties of a circular shape

(Appendix B.4). Only the centroid of the circle, the rotational center, was required in this process. The other image that contains the deposit was converted into a binary image for the next step.

4.5.3 Deposit thickness determination

There were several approaches to the deposition thickness discussed. As different methods would bring significant difference for the calculation, one of the methods need to be selected among the following approaches:

Direct measurement

Direct measurement measures the local deposit thickness h at point P by orienting a ray directly from the rotational center C (Figure 4.8a). As the most straightforward approach, it is only applicable under a condition of a circular-shaped mandrel with a rotation center at its centroid. Applying it in another condition would result in an error. An obvious case is indicated in Figure 4.8b. According to this approach, the observed thickness corresponding to two points along the same side is not the same on a square-shaped mandrel with a uniform deposit. Therefore, this method is not applicable in a general case.

(a)   (b)
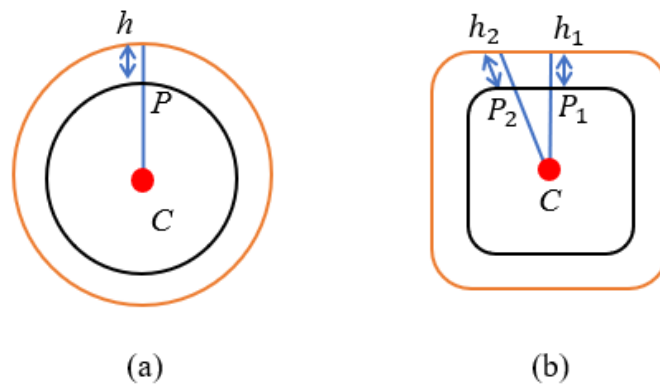
Figure 4.8. Direct measurement approach. (a) The approach is under the circular condition with

a rotational center at the centroid of the mandrel. (b) The approach is under the square-shaped mandrel with a rotational center at the centroid of the mandrel.

linear regression

In order to achieve a general approach, a linear regression method is created. Firstly, finding each point P corresponding to each degree of angle α (Figure 4.9a). A line perpendicular calculates the deposit thickness at the point to the linear regression through the point and (Figure 4.9b).

(a)   (b)
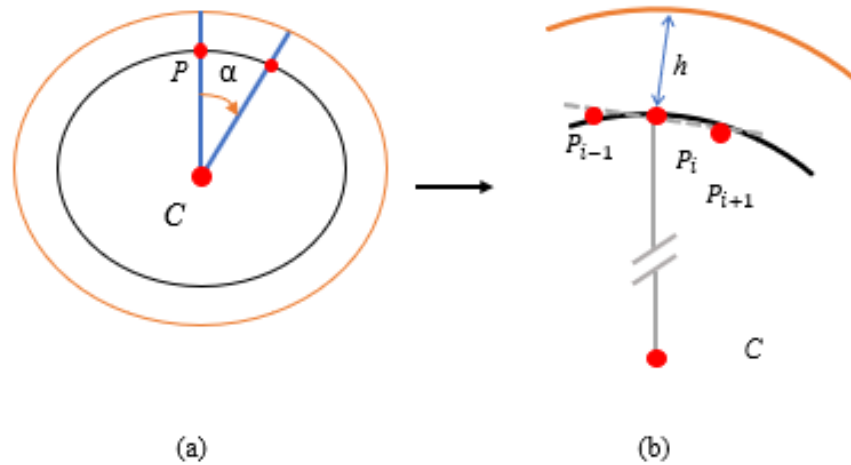
Figure 4.9. Linear regression approach. (a) Point P on the mandrel counted with angle α. (b) A detailed drawing for the linear regression approach.

Second-order curve fitting

This approach is similar to the linear regression approach. Instead of the thickness h being determined by a line perpendicular to the linear regression of three adjacent points, this method applies a second-order regression on the adjacent five points.

38

Eventually, the second-order curve fitting method is selected after applying this method in the programming. This approach is more applicable in the case of high surface roughness since two adjacent points around the selected point *P* are not symmetry around *P*. In the MATLAB program, this part had been separated into two functions: The linear scan function finding points P on the mandrel with the corresponding angle α (Appendix B.5). A regression and perpendicular line finding function is able to find the regression curve and the local perpendicular line on it (Appendix B.6). Finally, the thickness determination function determines the local thickness with the perpendicular line found in the previous step.

4.5.4 Algorithm Validation

To generally evaluate the precision of the MATLAB algorithm, a section of PVC tubing with an inside diameter of ¼'' and an outside diameter of ½'' was measured. The dimension is first verified with a caliper and then detected in the thickness determination MATLAB program. The result shows that the tubing thickness was detected correctly with a tolerance of four pixels (approximately 20µm with a magnification of 20x). For the deposit thickness of a complex shape, three to four points were sampled along the curve, and the deposit thickness of each point was first measured manually with the microscope. The thickness detected with the MATLAB program would be compared later to validate the preciseness of the detection.

5. Copper electroforming net shapes parts on additively manufactured mandrels

Electroforming is now one of the available manufacturing methods on the market. As electroforming is an atomic process, ideally, the formed structure is able to reach a precision with a tolerance of the size of the atom. While a non-uniform deposit can be commonly found on the electroformed parts caused by many reasons. Many methods were created to eliminate the non-uniform deposition, which is not cost efficient or time efficient. Instead of approaching to uniformness of the deposition, this chapter discusses one of the major factors that create non-uniform deposition and proposes an alternative solution—reshaping the mandrel at the beginning of the process. So that after the electroforming process, the manufactured parts can match with the desired shape upon the design.

On the other hand, electroforming provides us with an opportunity for high-aspect-ratio structure manufacturing. These structures and the thin-walled structures are commonly used in various industrial and engineering fields, such as XY micro-positioning stage. However, they are also difficult to fabricate with conventional manufacturing methods. In this study, a novel idea of various thickness deposition was brought up. The application of the electroforming procedures can be further expanded.

Towards Electroforming of Copper Net-shape Parts on Additively Manufactured Mandrels

Zhaohan Zheng[1], Rolf Wüthrich[1,2]

[1]*Department of Mechanical Industrial and Aerospace Engineering, Concordia University, 1455 De Maisonneuve Blvd. W. Montreal, Quebec, Canada H3G 1M8*

[2]*Department of Chemical and Materials Engineering, Concordia University, 1455 De Maisonneuve Blvd. W. Montreal, Quebec, Canada H3G 1M8*

5.1 Abstract

With the increasing demand for customization and personalization, the manufacturing industry faces new challenges related to cost-effective, low batch size production. Additive manufacturing (AM), which has an increasing share in the low-batch size production and rapid prototyping market, is among the most promising technologies to help to address this problematic but has some limitations in metal structure manufacturing. Post-processing is usually required to overcome high surface roughness, high porosity, and poor mechanical properties existing in the AM manufactured structures. Therefore, electroforming on an AM mandrel becomes a promising alternative solution for low batch production and complex structures with high aspect ratios. However, the uniformness,

deposition quality, and end-geometry of the electrodeposition on a mandrel are not always guaranteed. In this paper, a method is discussed to improve the geometric precision of the deposition on the mandrel, which calculates the mandrel geometry correction in order to achieve net-shape deposits. In addition, a method that allows the deposition of variable thickness on the same mandrel is proposed. As an application, a high aspect-ratio flexible structure is manufactured.

5.2 Introduction

Nowadays, the manufacturing industry faces new challenges due to the increased demand for low batch size production. Several drivers push towards low batch size production, among them just-in-time manufacturing [26] and the increased demand for customization and personalization of products by customers [25]. In most cases, the batch size of customized parts is very small [39]. The current manufacturing systems, designed for mass production, are no longer suitable for this emerging new reality [40]. Production of personalized products in small batch sizes comes with extra costs, compared to the production of mass produced and customized products, due to the design changes of the to-be-produced parts, making cost-effective, low batch size production challenging [41].

One of the most promising manufacturing technologies to address the needs of low batch size production is additive manufacturing (AM). Compared to conventional manufacturing, AM takes advantage of the freedom of part design which enables the manufacturing of large quantities of unique parts in a short lead time [42],[43]. However, direct metal printing systems come with a considerable investment and material cost because of special requirements for the raw material [44]. More dramatically, printed parts need a significant amount of post-processing to reach the

specified surface quality, geometry, and mechanical properties [24]. A further challenge is the production of thin-walled structures due to the layer-by-layer fabrication of parts. In fact, the manufacturing of metallic thin-walled structures is as well a challenge in conventional manufacturing. The level of difficulty increases with the aspect ratio [45]. Such structures are commonly used in various fields, such as aerospace and automotive, because of their lightweight and efficient energy absorption[31]. High-aspect-ratio thin-walled structures are as well commonly used as heatsinks or in flexures for micro positioning applications [46][47].

On the other hand, electroforming, traditionally used to form parts on mandrels, recently started to gain interest in academia as an alternative to direct metal printing [48]–[51]. The characteristic of electroforming can give a significant advantage in precision and thin-walled components production in comparison with other metal forming processes [52]. The idea proposed recently is to use filament 3D printing for a cost-efficient and time-efficient solution to produce personalized mandrels and subsequently electroplate them [51], [53]. This indirect manufacturing process is a potential solution for precise metal 3D parts fabrication with low energy consumption and low equipment investment costs, at least for some designs. As further electroforming results in higher quality surfaces than direct metal 3D printing, it can potentially address the issue of extensive post-processing [4], [51], [52].

However, electroforming has limitations too. Possible undesired voids build-up during the electroforming process will result in a rough and uneven surface with reduced mechanical properties. Further, the changing distance between the mandrel and the counter-electrode in complex geometries of the workpiece usually results in non-uniform thickness and undesired final geometry of the formed part [52]. Shields and baffles are traditionally used to address that problem [15], [54]. However, shields and baffles are not universal solutions and need to be designed

specifically for each mandrel geometry. They consequently add significant machining overhead for each design change.

This paper presents some solutions to increase the precision of the geometry of electroformed parts on 3D printed mandrels, avoiding shields and baffles. The key idea is to correct the mandrel geometry prior to printing so that after the electrodeposition process, the formed part has the desired geometry. The corrections are computed based on a simple mathematical model bringing only little manufacturing overhead related to design changes. Further, it is demonstrated how parts of variable thickness can be built, and as an application, a mechanical flexure of a high aspect ratio (1:90) is manufactured.

5.3 Experiment Setup

5.3.1 Mandrel Fabrication

Mandrels were designed in various shapes (Figure 5.1 a-c: circular shape, circular shape with four and eight sine waves superposed). Manufacturing was done using black ABS filaments on an Ultimaker 2+ FDM printer. After printing and cleaning the edges, the mandrel was wrapped with a thin copper foil and mounted on a copper rod (Figure 5.1 d). In order to deposit only on the side of the mandrel, epoxy and Teflon tape are applied on the top and bottom surface of the mandrel and other unwanted conductive surfaces.
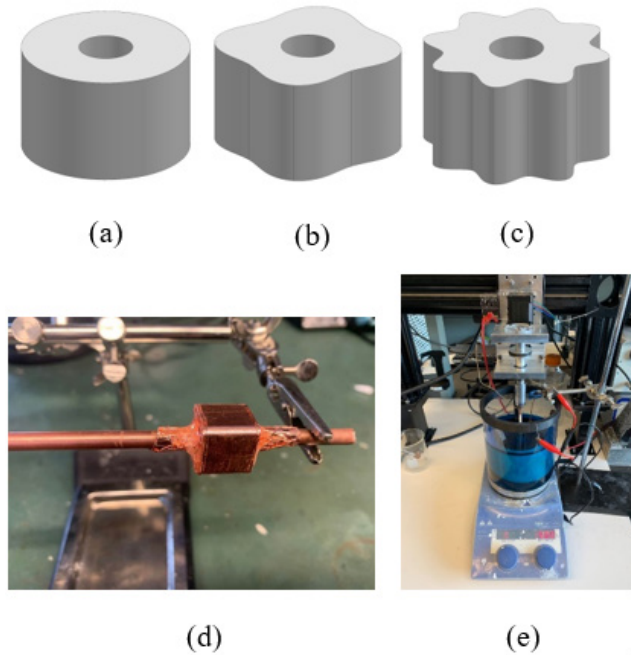
Figure 5.1. Mandrel shapes used in this study. (a) circular with a diameter of 16 mm (b) circular with four superposed sinewaves (c) circular with eight superposed sinewaves. (d) Mandrel mounted on copper axis and copper sheets on its surface (e) Overview of plating setup with mandrel mounted on the spindle.

5.3.2 Electroplating Process

The assembled mandrel is mounted on a spindle of the plating setup (Fig.51e). A circular-shaped copper sheet is used as a counter electrode, and a thin copper rod placed near the mandrel assembly serves as a pseudo-reference electrode. Electroplating was performed in a 1M Sulfuric Acid and 0.5M Copper Sulfate solution. Pulsed plating, where deposition pulses (at -150mV vs. Cu) and polishing pulses (at 100mV vs. Cu) were alternated, was used as described in [37].

Deposition pulses last until a charge of 2.7886 C/cm^2 was deposited (corresponding to a thickness of approximately 1 micron) and polishing pulses last for 10% of the deposition charge.

5.3.3 Deposition thickness determination

Following electroplating, the mandrel was removed from the spindle, rinsed with deionized water, and dried by blowing air on the surface. The plated mandrel was subsequently cold mounted in a reusable plastic mold (5 cm in diameter). The mounted samples were polished on a MetaServ 250 grinder, using 400 grid sandpapers to remove the material until the intersection of the mandrel and deposition were clearly revealed. The surface was further smoothened by repeated polishing with 600, 800, and 1200 grid sandpaper followed by a final polishing step with a 1µm MetaDi Polycrystalline Diamond Suspension polishing paste. Pictures of the polished sample cross-section were taken with a VHX-5000 microscope. Images were processed with MATLAB to characterize the contour and quantify the deposition thickness.

To determine the coordinates of the center of rotation of the mandrel, the coordinates of the centroid (coordinates determined with the built-in MATLAB function 'regionprops' from the Image toolbox) of the through-hole left in the mandrel after shaft removal were used (Fig.5.2a).

Afterward, to determine the thickness of the deposits, images were first converted into binary pictures. A ray originating from the mandrel's center of rotation (centroid of the through-hole left by the shaft) at an angle α with the x-axis was constructed (Fig.5.2b). The coordinates of the first color change detected alone the ray is recorded as a point P of the inner contour of the copper deposit. In order to measure the deposit thickness, the perpendicular distance to the mandrel from

point P to the outer contour is constructed (Fig.5.2c). Therefore, the osculating circle to the mandrel at point P is determined using two adjacent points to P. A line perpendicular to the tangent line of the osculating circle and passing through point P has an intersection with the outer contour of the deposition. The distance between this intersection and point P is considered as the deposit thickness.

(a)

(b)   (c)   (d)
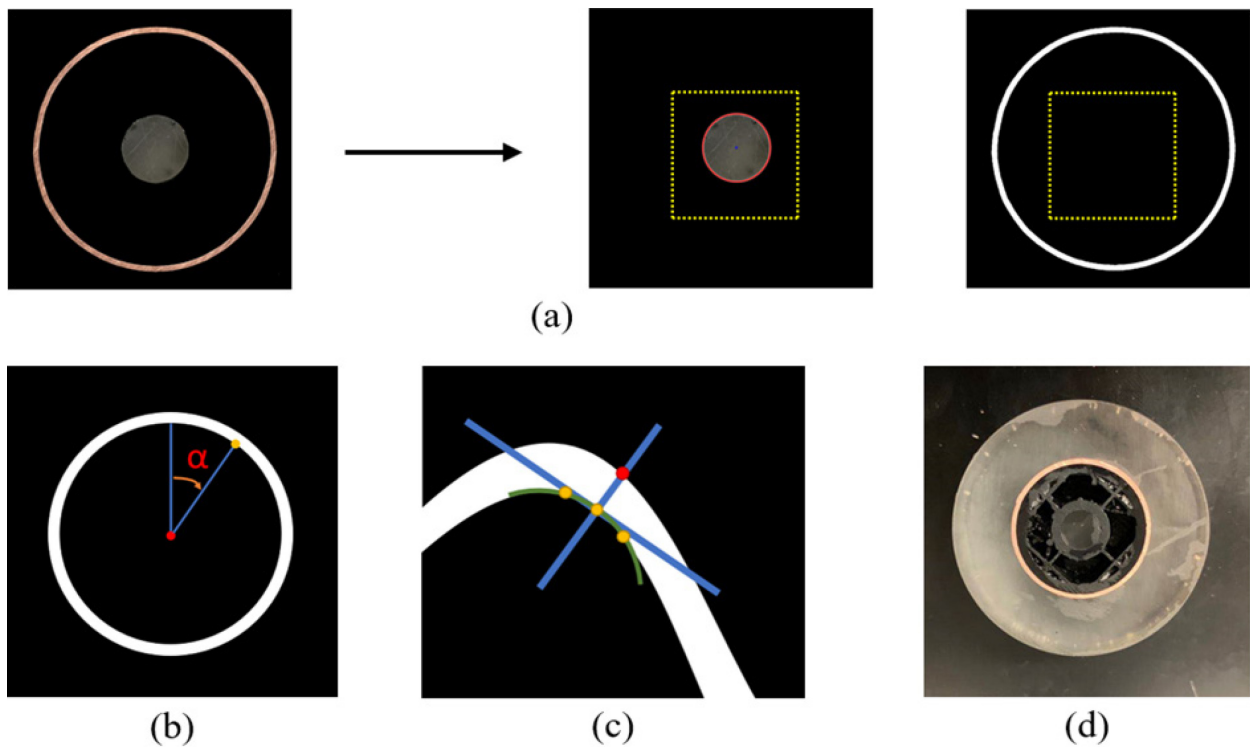
Figure 5.2. Image processing procedure. (a) image separation between opening from shaft and outer-shape (b) definition of angle α (c) schematic of the thickness calculation (d) polished sample.

5.4 Results

5.4.1 Correction for eccentrically mounted counter-electrodes

Electroforming is well suited to create uniform and homogenous deposits. However, a uniform deposition can only be guaranteed when a constant primary current density is applied to the mandrel surface. This is, for example, the case when a cylindrical mandrel is placed concentrically to a cylindrical counter-electrode. Fig.5.3a shows an example where a uniform copper layer of 400 µm was electroformed on a cylindrical mandrel.

(a)

(b)

(c)

48
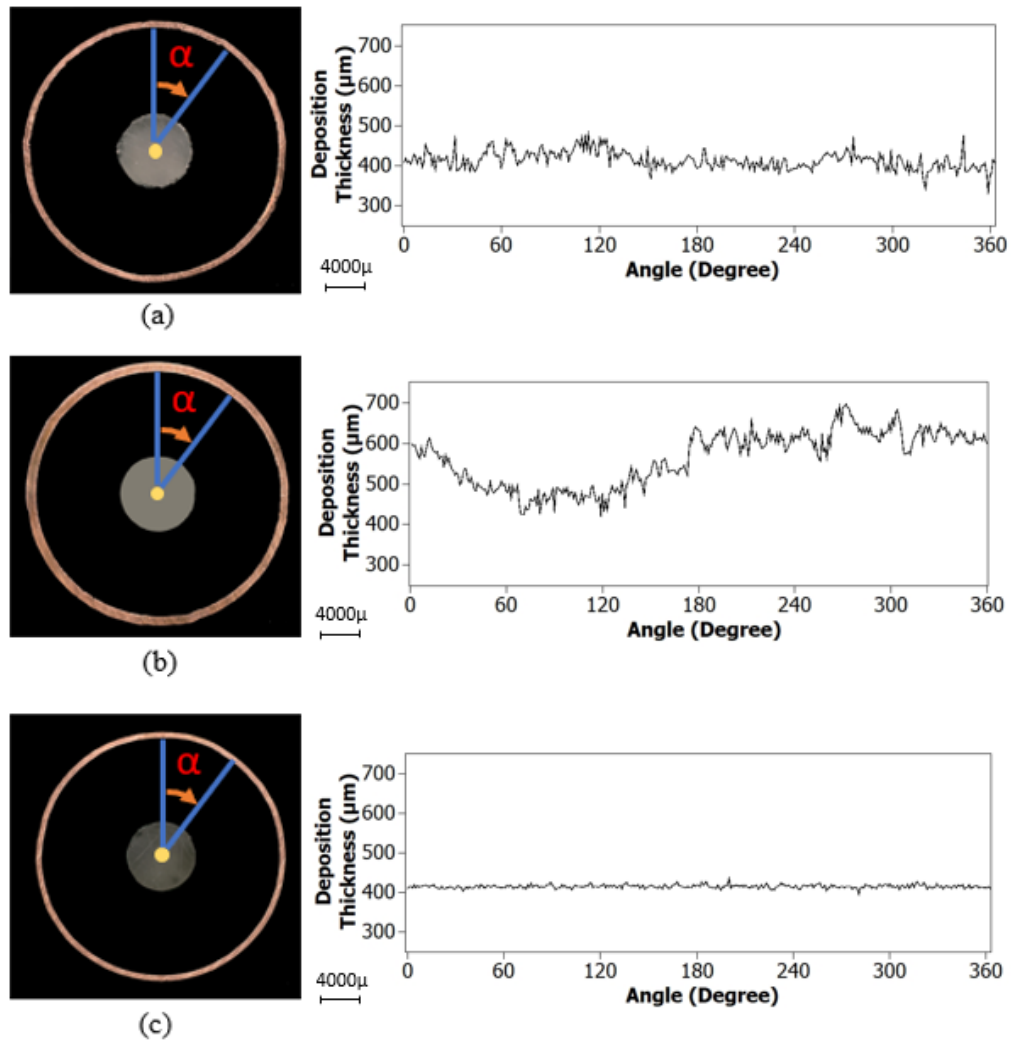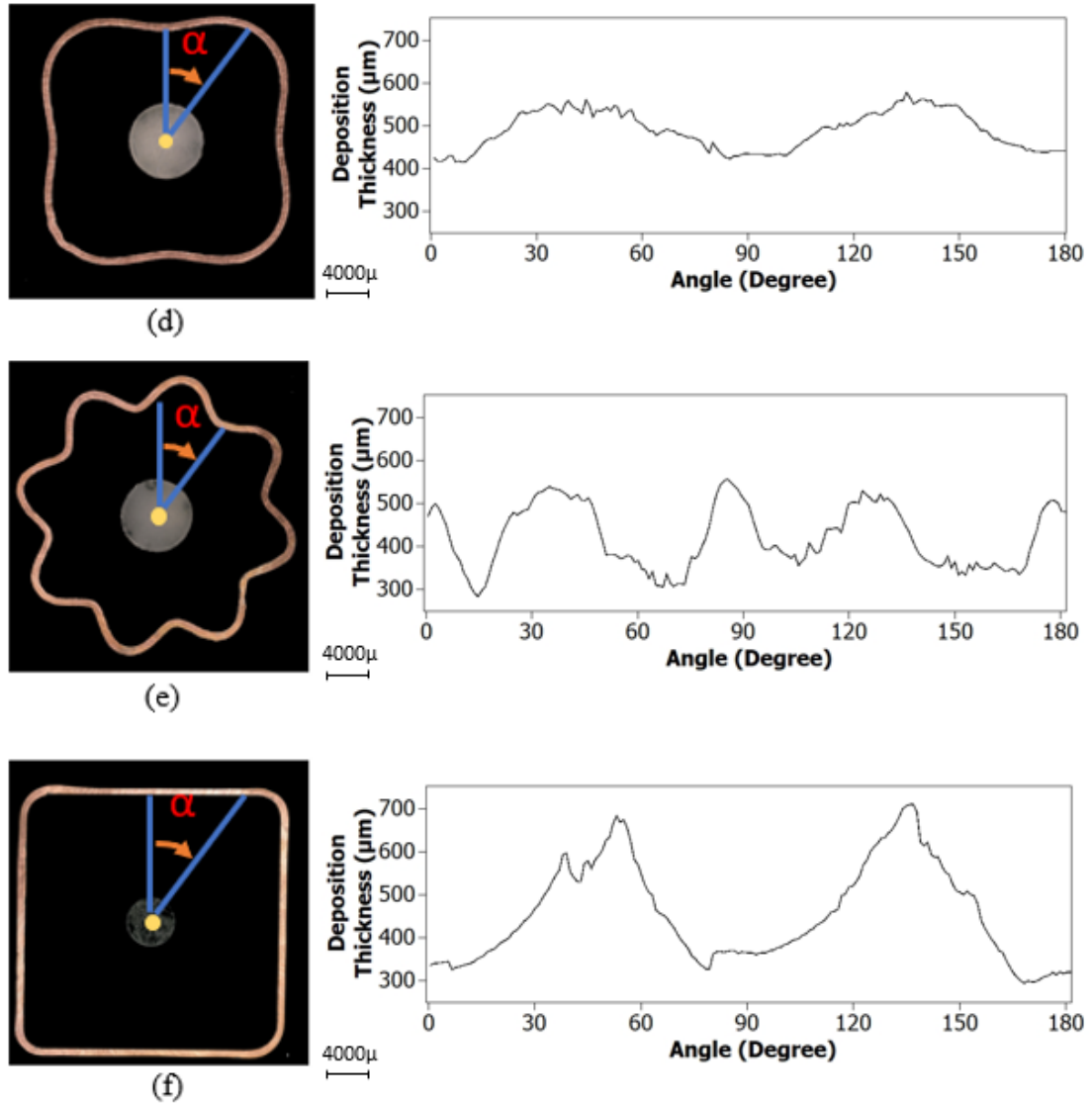
Figure 5.3. Microscope images of cross-sections and deposition thickness of electroformed coatings on various mandrels. (a) Circular mandrel (diameter of 16 mm) electroplated while concentrically placed relatively to a cylindrical counter electrode without rotation (b) Circular mandrel with a diameter of 16 mm electroplated when placed eccentrically (4 cm between rotation center and centroid of counter electrode) relatively to a cylindrical counter electrode without

rotation (c) Circular mandrel with a diameter of 16 mm electroplated when placed eccentrically (4 cm between rotation center and centroid of counter electrode) relatively to a cylindrical counter electrode with rotation (150 rpm) (d) Circular mandrel with four superposed sinewaves with rotation (150 rpm) (e) Circular mandrel with eight superposed sinewaves and rotation (150 rpm) (f) Square mandrel with rotation (150 rpm)

As On the other hand, as demonstrated in Fig.5.3b, placing a circular mandrel eccentrically relative to the counter electrode results in a non-uniform thickness due to the non-uniform primary current distribution on the mandrel surface. An average thickness of 500µm is obtained, but the deposit thickness is no longer uniform over the entire circumference.

The misalignment between a symmetric mandrel and a symmetric counter electrode can be corrected by a straightforward approach using mandrel rotation. Rotating (150 rpm) the circular mandrel around its symmetry axis can result in a uniform thickness even if placed eccentrically relatively to the counter electrode (Fig.5.3c). This can be readily understood as rotating the mandrel will average the non-uniform current density on the mandrel surface over time [24].

However, when the mandrel is not a cylindrical shape, as in Fig.5.3d, 5.3e, and 5.3f, a uniform deposit can no longer be achieved, even with rotation around the symmetry axis of the mandrel. Indeed, the distance from the mandrel surface to the center of rotation is no longer constant. Adding rotation will correct for an eccentrically mounted mandrel relative to the counter-electrode. However, the variations of distances from the mandrel surface to the axis of symmetry cannot be averaged out. For example, in both cases, Fig.5.3d and 5.3e, an average thickness of 450µm is achieved, but the superposition of the sine waves can be clearly seen. In case Fig.5.3f, where the

distance from mandrel surface to counter-electrode varies more than in cases Fig.5.3d and 5.3e, the variations in deposit thickness are larger.

5.4.2 Correction of mandrel shape

In several applications, a uniform deposit thickness is not essential, but the final outer shape of the formed part is the target. The advantage of 3D printing the mandrel is that, in principle, one can print a mandrel shape such that after electroforming, the resulting part has the desired shape. As shown by the simple experiments with mandrel rotation, the non-uniformity of the primary current distribution due to an eccentrically mounted mandrel (relatively to the center of the counter-electrode) can be corrected. However, the variations from the mandrel surface to the center of rotation result in variable deposit thickness with the consequence that the mandrel geometry to obtain a given target part needs to be calculated.

.
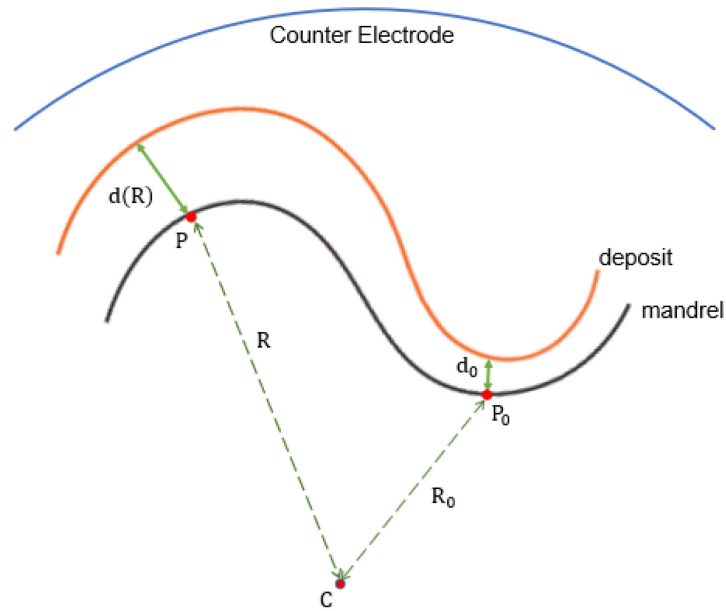
Figure 5.4: Variation of deposition thickness on a mandrel. Point C is the center of the cylindrical counter-electrode.

As the deposition thickness is governed by the primary current distribution[25], the geometric distance from the mandrel surface to the counter electrode results in a non-uniform current distribution. As the distance R from a point P on the mandrel surface to the center C of the cylindrical counter-electrode changes, the deposition thickness $d(R)$ in P will also change (Fig.5.4). Assuming as a first approximation a linear dependence, one can write:

$$d(R) = d_o + k(R - R_0) \qquad \text{Eq. 5.1}$$

with d_o the thickness of the deposit in a reference point P_o at a distance R_o from C. The positive parameter k will have to be determined experimentally.
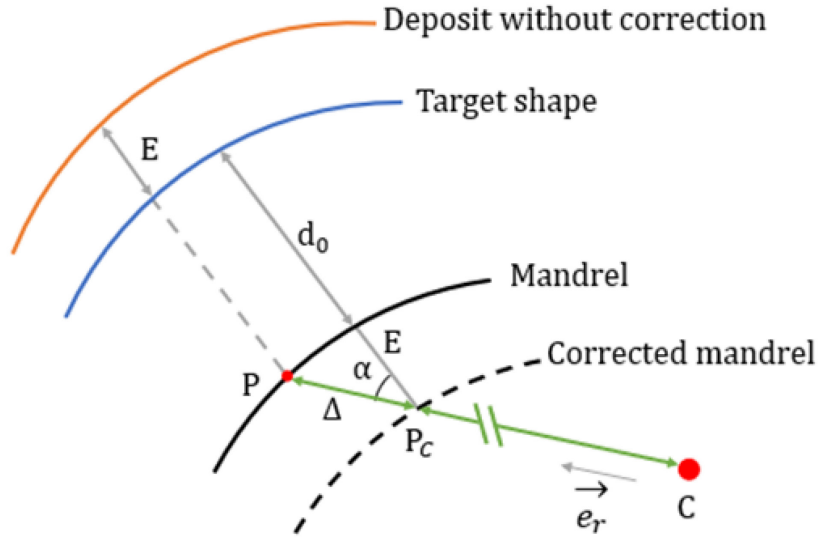
Figure 5.5: Geometry of initial mandrel and corrected mandrel. Refer to text for the explanation of the various symbols.

Eq.1, together with the experimentally determined coefficient k, allows calculating a mandrel shape such that, after electroforming, the resulting outer surface follows the targeted shape. In the following this mandrel will be referred as the "corrected mandrel". Note that the deposition thickness will not be uniform after electroforming on the corrected mandrel but varies around an average thickness d_o. However, the outer shape of the formed part will have the targeted shape.

To compute the corrected mandrel, one starts from an initial mandrel which has the same shape as the targeted one, minus the distance d_o, the desired average deposition thickness (Fig.5.5). Consider a point P on the initial mandrel. Using Eq.1, the error E between the deposited thickness $d(R)$ and the desired thickness d_o can be written as

$$E = d(R) - d_o = k(R - R_0)$$ Eq.2

where R is the distance between P and C, and R_0 is the distance between P_o and C.

These differences E are used to determine the corrections to be applied to the initial mandrel. The corrected point P_c is obtained by moving point P along the line from point P to the center C of the counter-electrode:

$$\overrightarrow{CP_c} = \overrightarrow{CP} - \Delta \vec{e}_r$$ Eq.3

where $\vec{e}_r$ is a unit vector pointing from the counter-electrode center C to point P. The distance Δ is calculated as:

$$\Delta = \frac{E}{cos(\alpha)}$$ Eq.4

where α is the angle between the vector $\overrightarrow{CP}$ and normal vector to the mandrel at point P. The change in location from point P to P_C will result in a variation in the deposition thickness, but the outer shape will be of the desired target shape.

In this study, the coefficient k is determined from deposition experiments shown in Fig.5.3d and 5.3e. For each point on the mandrel surface, the coefficient k_i is calculated from Eq.2 as

$$k_i = \frac{d_i - d_0}{R_i - R_0}$$

Eq.5

where R_0 is the mandrel radius when the angle α has a value of zero (Fig.5.2b), d_0 is the corresponding deposit thickness, R_i and d_i are the mandrel radius and deposit thickness at an angle α (measurements were done for increments of one degree).

The average value of the k_i calculated from Fig.5.3d and 5.3e is used as the value for the coefficient k for this study. A value of 0.05 ± 0.01 is found.
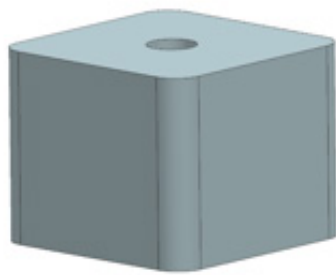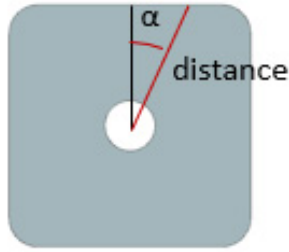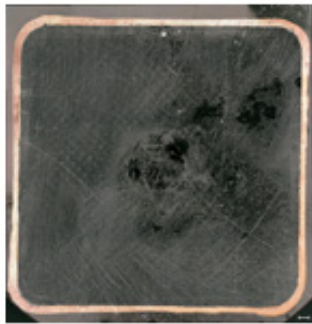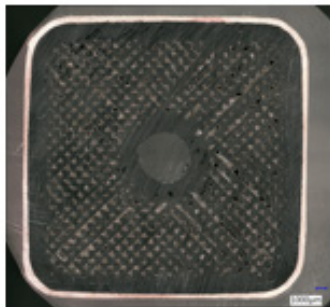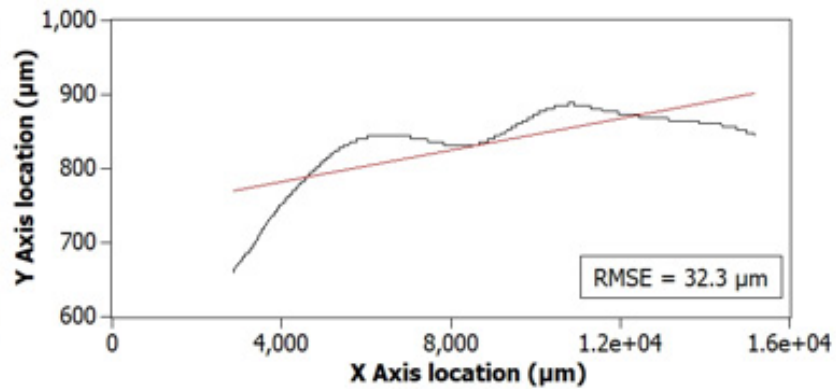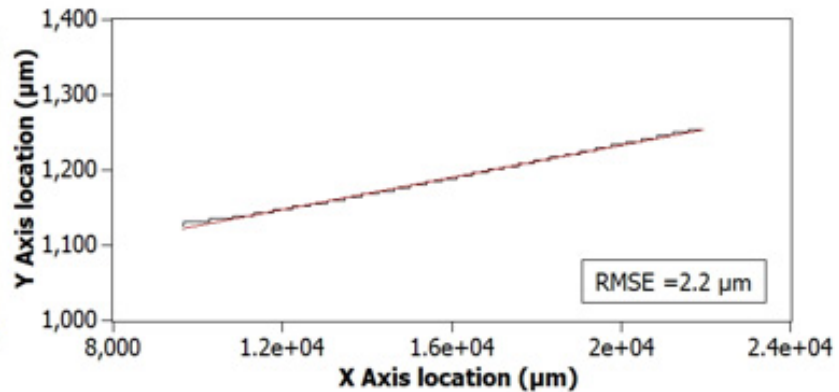
Figure 5.6: Electroforming of a square shape on a 3D printed mandrel. (a) Target final square shape. (b) Top view of mandrel without correction. (c) Top view of the mandrel with correction. (d) Plating result on the uncorrected mandrel with linear regression and RMSE value of the top edge of deposit on the uncorrected mandrel. (e) Plating result on the corrected mandrel with linear regression and RMSE value of the top edge of deposit on the corrected mandrel.
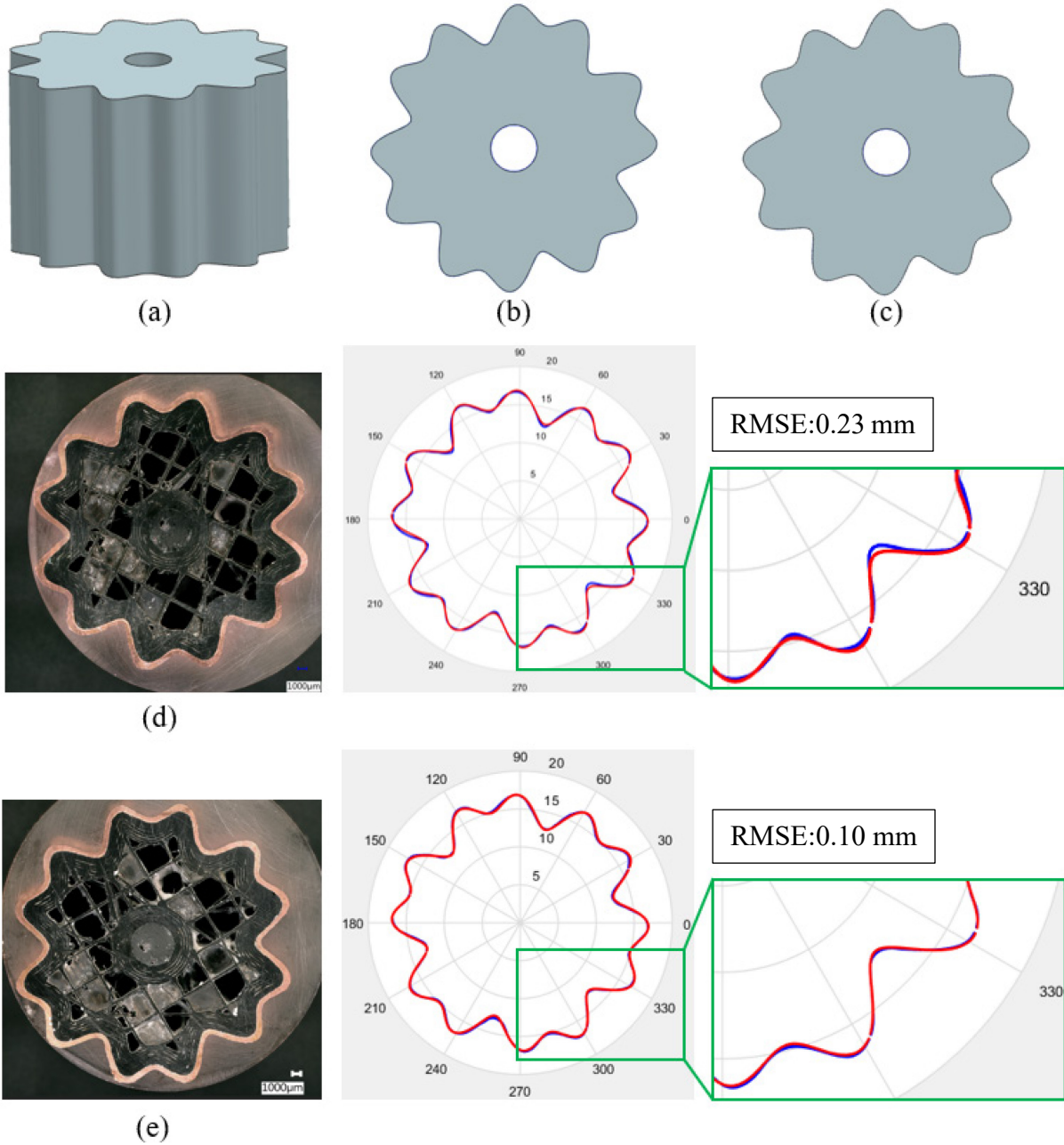
Figure 5.7: Electroforming of a target shape with equation $0.7(2 - 0.15 \sin 6\theta + 0.2 \cos 12\theta)$ [cm]. (a) Target final shape. (b) Top view of mandrel without correction. (c) Top view of the mandrel with correction. (d) Plating result on the uncorrected mandrel with curve fit (red curve target shape and blue curve actual deposit) and RMSE value of the deposit on the uncorrected

mandrel. (e) Plating result on the corrected mandrel with curve fit (red curve target shape and blue curve actual deposit) and RMSE value of the deposit on the corrected mandrel.

5.4.3 Experimental validation of mandrel correction computations

To validate the feasibility of the proposed approach to compute the corrected mandrel geometry, a square mandrel (Fig.5.6) and a complex-shaped mandrel (Fig.5.7) are created. Fig.5.6c and 5.7c show the computed mandrel by the methodology described above.

Fig.5.6d and 5.6e display the coordinates of one of the four faces of the electroformed part. Performing linear regression on these coordinates and computing the root mean square error (RMSE) demonstrates the efficient correction process (reduction from about 32µm to about 2 µm).

The correction method is not only efficient for square shapes but also for more complex shapes, as illustrated in Fig.5.7. After correction, Fig.5.7d and 5.7e show that the deposit has a contour fitting better the target shape than the one without correction (RMSE error decreased form 0.23mm to 0.1mm). In summary, after applying the algorithm to correct the mandrel, the outer shape of the electroformed part can be controlled, and the method is suitable for both simple and complex shapes.

However, this correction method has its limitation too. By comparing the results from the parts of Fig.5.6 and Fig.5.7, it is observed that this method gives a better correction for the square-shaped mandrel than for the mandrel with a complex-shaped contour. On none-straight portions of the mandrel (peaks and valleys), the correction is less accurate. As evidenced from the zoomed view of the actual deposit and targeted shape shown in Fig.5.7e, non-straight portions contribute

significantly more to the error than the rest of the shape. This comes from the assumption that the correction is essentially linear in the distance variation compared to a reference distance (Eq.1).

5.4.4 Multiple thicknesses of electroformed parts

Some applications require that the formed part has various thicknesses and not only a single average constant thickness. This last set of experiments demonstrates that it is possible to electroform on mandrels, having an extruded type of geometry, parts with different thicknesses in the same design.

The idea to achieve various thickness depositions is illustrated in Fig.5.8. Initially, the mandrel is designed in a multi-level structure with specific portions of the mandrel surface covered by a conductive copper layer (Fig.5.8a). Initially, the electrodeposit is only created on the lower-level surface (Fig.5.8b). Electrical connection between the top surface and the working electrode is established as soon as the deposit rises to the same level as the conductive surface on the higher level (Fig.5.8c). The entire surface will now see an electroformed layer growing on it (Fig. 5.8d). The finished part is the complementary shape of the mandrel (Fig.5.8e).
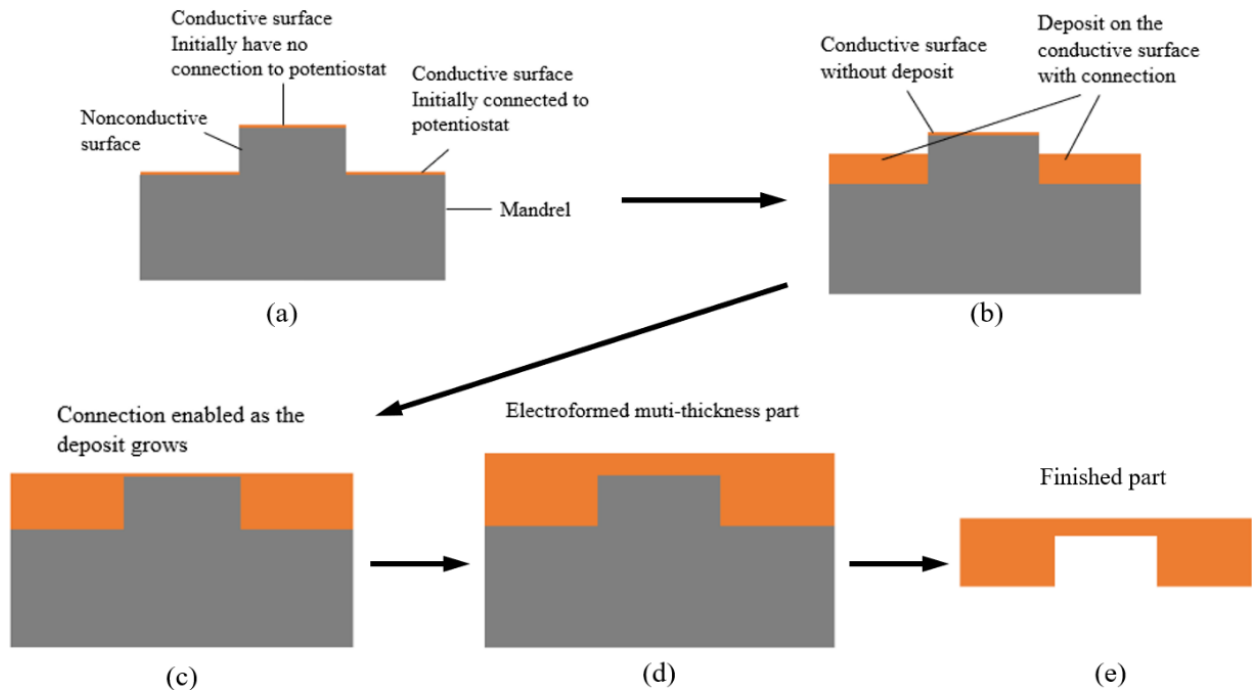
Figure 5.8: General idea of the varied-thickness electroforming process. (a) Mandrel design. (b) Initial deposit on the mandrel. (c) Deposit enables the connection between the different surface levels. (d) Completed deposition on the mandrel. (e) Finished part after mandrel removal.
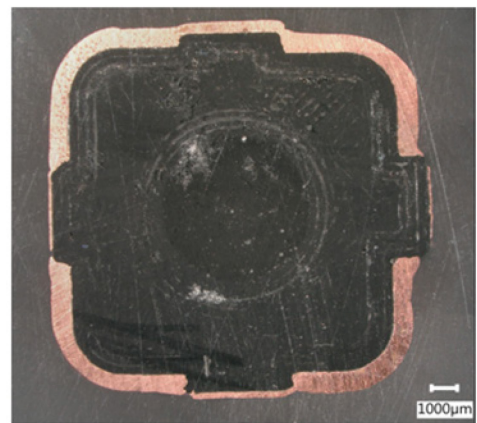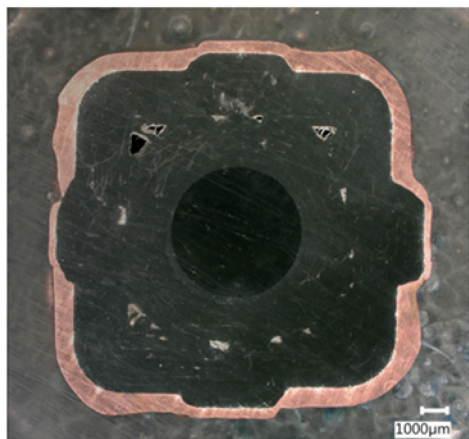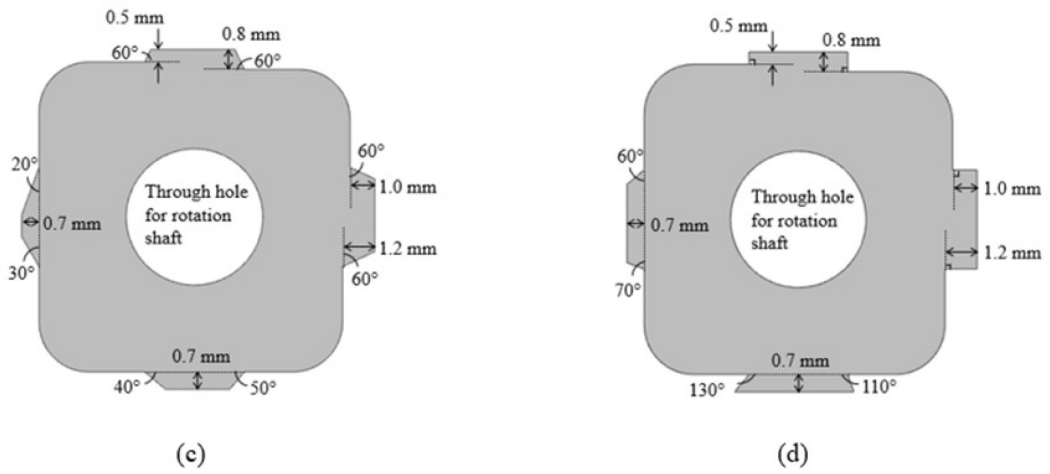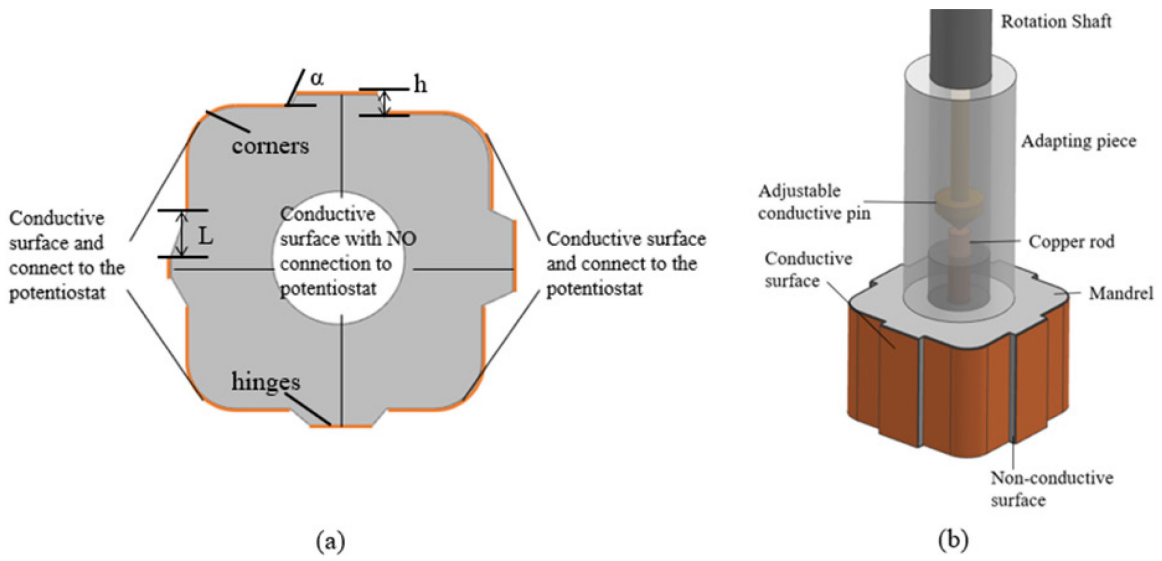
Figure 5.9: Multiple deposit thicknesses mandrel designs. (a) General geometry and definitions

of parameters of the mandrel to establish design rules. (b) Assembly of mandrel on shaft. (c) and (d) top views of mandrel designs. (e) and (f) electroformed mandrel corresponding to the mandrels (c) and (d).

In order to establish design rules for the implementation of the method of Figure 5.8, two mandrels are designed with different angles α and height changes h (Figure 5.9(b), (c)). Electroforming was performed with mandrel rotation of 300 rpm.

Electroforming experiments show that for angles α smaller than 50° (Fig. 5.9e), deposits tend to climb on the non-conductive surface and enable the connection earlier than desired. This results in an outer shape that is not flat but presents an "outgrowth". When the angle α is too small (smaller than 20°), a disconnection happens because of the long non-conductive distance, forming an incomplete structure.

For stiffer angles (larger than 60°, Fig.5.9f) the "outgrowth" formation can be avoided, and the finished part has a leveled surface. An angle of 90° is too stiff, as seen in the right side of the formed deposit of Fig.5.9f. The lower-level deposit does not climb perpendicular to the "outgrowth", but on the contrary, tends to grow in a circle type geometry. An intermediate angle of 70° is optimal, as seen on the left side of the formed deposit of Fig.5.9f. A level final surface is achieved.
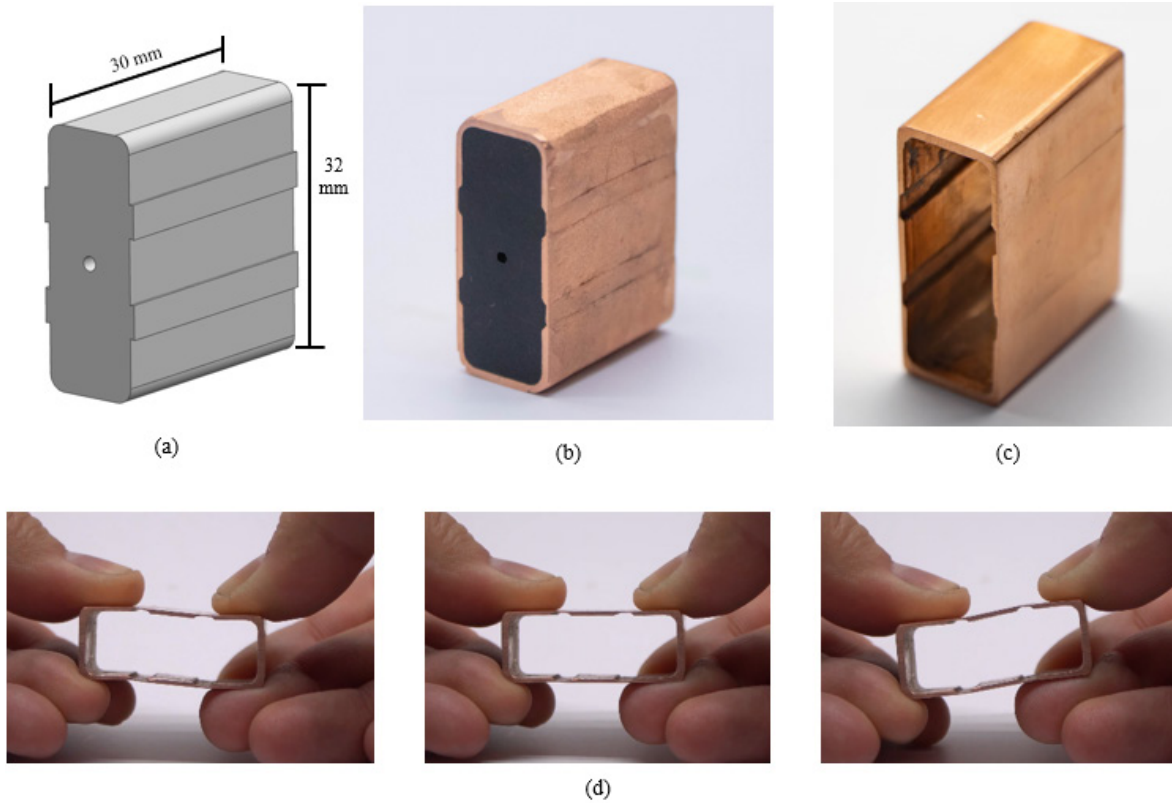
Figure 5.10: Various thicknesses mandrel deposition example. (a) Designed mandrel. (b) mandrel after the electroforming. (c) The polished copper part after the ABS mandrel has been removed. (d) demonstration of the structure flexibility.

To demonstrate an application of the developed method, a high aspect ratio flexure was manufactured. Fig.5.10 shows the design and the electroformed part. Prior to removing the ABS mandrel, some hand polish on the outer surfaces was applied Fig.5.10c. The manufactured part has a hinge thickness of 0.3 mm with a height of 27mm. This allows to achieve good flexibility and can be easily deformed by hand (Fig.5.10d). The aspect ratio of the hinges is about 1:90. It is worth mentioning that this aspect ratio can, in principle, be extended much higher, as it is only limited by the length of the mandrel. Consequently, the aspect ratio of the fabricated structures is

determined by the capability to manufacture mandrel surfaces straight enough over their entire length.

5.5 Further Application

A further application of the various thickness electroformed structures can be developed. Since electroforming is an additive process, theoretically, a design with any aspect ratio can be created. The aspect ratio of the fabricated structures is only limited by the mandrel surface and the number of electroforming pulses that control the thickness of the deposition. Same as thin-walled structures, the wall thickness can be simply adjusted by the forming time. Therefore, the structures such as flexure mechanisms can be fabricated with the provided method. Some compliant stages are commonly used as micro-positioning motion control. For example, the XY positioning stages are one of the most crucial components in robotics. Also, the stabilizing system for the vibration isolation tables served some unique instruments, microscope, for example. Other thin-walled structures include different kinds of sensors that can also be fabricated with electroforming for better precision.

5.6 Conclusion

In this study, the non-uniform deposition problem in electroforming on additively manufactured ABS mandrels is addressed. By mounting the mandrel on a spindle, it is possible to obtain a process that is not sensitive to the relative location of the cylindrical counter-electrode and the mandrel. Regardless of the relative position of mandrel and counter-electrode, the same deposition geometry

is obtained. However, mandrel rotation does not avoid the formation of non-uniform deposition layer thickness.

In applications, the uniformity of the deposition layer is often less important than the geometry of the outer shape. Therefore, instead of investing in a method to achieve a uniform thickness of the deposition layer, it appears more interning to develop a methodology to correct the mandrel geometry in order to achieve, after electroforming, the target geometry of the part. The proposed correction method was validated on various geometries. A root-mean-square error of 100 $\square$m or less can be achieved on the final part geometry.

Furthermore, a methodology to build parts with a varied-thickness structure is presented. As a potential application, a high aspect ratio (1:90) thin-walled flexible structure was manufactured.

6. Conclusion and Future Work

The study discussed the non-uniform deposition of the electroforming on an AM manufactured mandrel and aimed to eliminate the effect of the thickness variation. In the case of the circular-shaped mandrel, placing the mandrel eccentrically in a circular-shaped counter-electrode can result in a non-uniform deposit on the mandrel. The variation of the deposit thickness can be easily eliminated by applying rotation with a proper speed on the mandrel. When it comes to a more complex shape, only the rotation on the mandrel is not sufficient to eliminate the deposition variation. The processed data shows a linear relationship can be assumed between the deposition thickness and the local radius of each point on the mandrel contour. The thickness of the deposition becomes predictable with the aid of the linear relationship assumption, which also enables the proper modification of the mandrel based on this assumption. Therefore, the finished outer contour of the mandrel can be adequately controlled. Instead of the other method that forces the deposition uniformness, the mandrel with modification can be easily applied in mass production as it has no specific requirement to the other electrochemical cell components. At the same time, it helps the finished structure in a more practical way to follow the original design properly. Several results with different mandrel shapes demonstrated that the deposited part followed the original design better than the sample without correction after the mandrel modification.

The second part of the study provides an alternative idea for high-aspect-ratio thin-walled structure manufacturing since the EDM process and direct metal printing have their own

limitations. The combination of the electroforming and AM mandrel provide more possibility for those complex structures. The process is able to fabricate a thin wall flexible structure as the demonstration.

In future research, the possibility of multiple identical part deposition and diverse parts depositions needs to be further discovered. Mass customization can be achieved by electroforming a significant quantity of the parts simultaneously. Nevertheless, it also requires several specific adjustments for each part based on its geometric size and designed forming thickness. Automatic control can be further implemented on the system to reach a finer surface roughness and a better geometric precision. On the other hand, the multi-thickness mandrel design for the thin-walled structure can be further developed and refined based on the application. The multi-level design should not be limited only to thin-walled structures fabrication but can be applied to other complex structures fabrication that needs to be further discussed.

References

[1]   I. Gibson, D. W. Rosen, and B. Stucker, *Additive Manufacturing Technologies: Rapid Prototyping to Drect Digital Manufacturing*. 2010.

[2]   V. S. Bagotsky, *Fundamentals of Electrochemistry*, vol. 5, no. March. 2006.

[3]   P. Vaýsek, "Principles of Electrochemistry, 2nd edition," *Bioelectrochemistry Bioenerg.*, vol. 33, no. 1, pp. 107–108, 1994.

[4]   M. Schlesinger and M. Paunovic, *Modern Electroplating*. 2010.

[5]   I. S. Brandt, M. A. Tumelero, S. Pelegrini, G. Zangari, and A. A. Pasa, "Electrodeposition of Cu2O: growth, properties, and applications," *J. Solid State Electrochem.*, vol. 21, no. 7, pp. 1999–2020, 2017.

[6]   N. Kanani, *Electroplating*. 2004.

[7]   C. M. A. Brett and A. M. O. Brett, *Electrochemistry: Principles, methods, and applications*. 1993.

[8]   D. Landolt, "Mass Transport in Pulse Plating.," *Theory Pr. Pulse Plat.*, no. January 1986, pp. 55–71, 1986.

[9]   V. M. Volgin and A. D. Davydov, "Calculation of limiting current density of metal electrodeposition on vertical plane electrode under conditions of natural convection," *Electrochim. Acta*, vol. 49, no. 3, pp. 365–372, 2004.

[10]   C. Lefrou, P. Fabry, and J.-C. Poignet, *Electrochemistry: The basics, with Examples*. 2009.

[11]   G. Inzelt, A. Lewenstam, and F. Scholz, *Handbook of reference electrodes*. 2013.

[12]   Y. J. Tan and K. Y. Lim, "Understanding and improving the uniformity of electrodeposition," *Surf. Coatings Technol.*, vol. 167, no. 2–3, pp. 255–262, 2003.

[13]   J. M. Yang, D. H. Kim, D. Zhu, and K. Wang, "Improvement of deposition uniformity in alloy electroforming for revolving parts," *Int. J. Mach. Tools Manuf.*, vol. 48, no. 3–4, pp. 329–337, 2008.

[14]   D. S. Solovjev, I. A. Solovjeva, V. V. Konkina, and Y. V. Litovka, "Improving the uniformity of the coating thickness distribution during electroplating treatment of products using multi anode baths," *Mater. Today Proc.*, vol. 19, pp. 1895–1898, 2019.

[15]   E. C. Knill, "Effects of shields and baffles on the distribution of chromium electrodeposits," *Plat. Surf. Finish.*, vol. 76, no. 3, pp. 38–45, 1989.

[16]   E. C. Knill, "The Effects of shields and baffles on the distribution of chromium electrodeposits," *Plat. Surf. Finish.*, vol. 76, no. 3, pp. 38–45, 1989.

[17]   A. Gebhardt, *Understanding Additive Manufacturing*. 2011.

[18]   A. Bandyopadhyay and S. Bose, *Additive Manufacturing*. 2016.

[19]   T. Gornet, "History of Additive Manufacturing," pp. 1–24, 2017.

[20]   T. J. Phillips and J. S. Dover, "A Brief History of Additive Manufacturing and the 2009 Roadmap for Additive Manufacturing: Looking Back and Looking Ahead," *US-Turkey Work. Rapid Technol.*, vol. 24, no. 24, pp. 5–11, 2009.

[21]   D. T. Pham and R. S. Gault, "A comparison of rapid prototyping technologies," *Int. J. Mach. Tools Manuf.*, vol. 38, no. 10–11, pp. 1257–1287, Oct. 1998.

[22]   P. Stavropoulos and P. Foteinopoulos, "Modelling of additive manufacturing processes: A review and classification," *Manuf. Rev.*, vol. 5, 2018.

[23]   K. Kun, "Reconstruction and development of a 3D printer using FDM technology," *Procedia Eng.*, vol. 149, no. June, pp. 203–211, 2016.

[24]   W. E. Frazier, "Metal additive manufacturing: A review," *J. Mater. Eng. Perform.*, vol. 23, no. 6, pp. 1917–1928, 2014.

[25]   O. Okhiria, "Cost Management in the New Product Introduction Process of TruPrint 1000," 2017.

[26]   Y. Monden, *Toyota Production System*. 1994.

[27]   B. J. Pine, "Mass Customisation: The New Frontier in Business Competition," *Aust. J. Manag.*, vol. 17, no. 2, pp. 271–283, Dec. 1993.

[28]   D. L. Bourell, "Perspectives on Additive Manufacturing," *Annu. Rev. Mater. Res.*, vol. 46, pp. 1–18, 2016.

[29] R. Leach and S. Carmignato, *Precision Metal Additive Manufacturing*. CRC Press, 2021.

[30] Y. Huang, M. C. Leu, J. Mazumder, and A. Donmez, "Additive manufacturing: Current state, future potential, gaps and needs, and recommendations," *J. Manuf. Sci. Eng. Trans. ASME*, vol. 137, no. 1, pp. 1–10, 2015.

[31] N. Ahmed, M. A. Naeem, A. U. Rehman, and M. Rafaqat, "High aspect ratio thin-walled structures in d2 steel through wire electric discharge machining (EDM)," *Micromachines*, vol. 12, no. 1, pp. 1–21, 2021.

[32] S. E. Alkhatib, F. Tarlochan, A. Hashem, and S. Sassi, "Collapse behavior of thin-walled corrugated tapered tubes under oblique impact," *Thin-Walled Struct.*, vol. 122, no. January, pp. 510–528, 2018.

[33] P. Bałon *et al.*, "The application of thin-walled integral constructions in aviation as exemplified by the SAT-AM project," *MATEC Web Conf.*, vol. 304, p. 01026, 2019.

[34] A. C. Kermode, R. H. Barnard, and D. R. Philpott, *Mechanics of Flight*. 2006.

[35] H. Marashi, A. A. D. Sarhan, I. Maher, and M. Sayuti, "Techniques to Improve EDM Capabilities: A Review," *Compr. Mater. Finish.*, vol. 1–3, pp. 171–202, 2017.

[36] Z. Wu, S. P. Narra, and A. Rollett, "Exploring the fabrication limits of thin-wall structures in a laser powder bed fusion process," *Int. J. Adv. Manuf. Technol.*, vol. 110, no. 1–2, pp. 191–207, 2020.

[37] P. Fallah, "Fabrication and optimization of 3D metallic parts using electroplating of

additively manufactured parts," 2018.

[38]   R. Wuthrich, "ECTk." 2013.

[39]   B. J. Pine, *Mass Customization: The New Frontier in Business Competition*. Boston, MA: Harvard Business School Press, 1993.

[40]   S. J. Hu, "Evolving paradigms of manufacturing: From mass production to mass customization and personalization," *Procedia CIRP*, vol. 7, pp. 3–8, 2013.

[41]   D. G. Reinertsen, *The principles of Product Development Flow*. .

[42]   D. S. Thomas and S. W. Gilbert, "Costs and cost effectiveness of additive manufacturing: A literature review and discussion," *Addit. Manuf. Costs, Cost Eff. Ind. Econ.*, pp. 1–96, 2015.

[43]   T. Duda and L. V. Raghavan, "3D Metal Printing Technology," *IFAC-PapersOnLine*, vol. 49, no. 29, pp. 103–110, 2016.

[44]   T. DebRoy, T. Mukherjee, J. O. Milewski, and J. W. Elmer, "Scientific, technological and economic issues in metal printing and their solutions," *Nat. Mater.*, vol. 18, no. 10, pp. 1026–1032, 2019.

[45]   B. Bhattacharyya, *Electrochemical Micromachining for Nanofabrication, MEMS and Nanotechnology*. Elsevier Inc., 2015.

[46]   C. Lee and J. A. Tarbutton, "Compliance and control characteristics of an additive manufactured-flexure stage," *Rev. Sci. Instrum.*, vol. 86, no. 4, 2015.

[47] P. Gräser, S. Linß, F. Harfensteller, and M. Torres, "High-precision and large-stroke XY micropositioning stage based on serially arranged compliant mechanisms with flexure hinges," *Precis. Eng.*, vol. 72, no. February, pp. 469–479, 2021.

[48] Y. Wu, S. Qian, H. Zhang, and Y. Zhang, "Experimental study on three-dimensional microstructure copper electroforming based on 3D printing technology," *Micromachines*, vol. 10, no. 12, 2019.

[49] R. Matsuzaki, T. Kanatani, and A. Todoroki, "Multi-material additive manufacturing of polymers and metals using fused filament fabrication and electroforming," *Addit. Manuf.*, vol. 29, no. February, p. 100812, 2019.

[50] G. S. Phull, S. Kumar, R. S. Walia, and H. Singh, "Copper Electroforming Optimization for Fused Deposition Modeling Produced ABS Components for Indirect Tooling Applications," *J. Adv. Manuf. Syst.*, vol. 19, no. 1, pp. 15–29, Mar. 2020.

[51] M. Sugavaneswaran, M. T. Prince, and A. Azad, "Effect of electroplating on surface roughness and dimension of FDM parts at various build orientations," *FME Trans.*, vol. 47, no. 4, pp. 880–886, 2019.

[52] J. A. MacGeough, M. C. Leu, K. P. Rajurkar, A. K. M. De Silva, and Q. Liu, "Electroforming process and application to micro/macro manufacturing," *CIRP Ann. - Manuf. Technol.*, vol. 50, no. 2, pp. 499–514, 2001.

[53] A. E. W. Rennie, C. E. Bocking, and G. R. Bennett, "Electroforming of rapid prototyping mandrels for electro-discharge machining electrodes," *J. Mater. Process. Technol.*, vol. 110,

73

no. 2, pp. 186–196, 2001.

[54] U. Pilz, "Calculation of the parameters of perforated shields for applications in electroforming," *Plat. Surf. Finish.*, vol. 82, no. 12, pp. 56–57, 1995.

[55] Y. S. Dong, P. H. Lin, and H. X. Wang, "Electroplating preparation of Ni-Al2O3 graded composite coatings using a rotating cathode," *Surf. Coatings Technol.*, vol. 200, no. 11, pp. 3633–3636, 2006.

Appendix A: Motor Rotation Control with Raspberry Pi 3 B+

```python
from time import sleep
import RPi.GPIO as GPIO

GPIO.setwaringins(False)
GPIO.setmode(GPIO.BOARD)

DIR = 7
STEP = 11
feq = 100000
DUTY_F = 30

GPIO.setup(DIR, GPIO.OUT)
GPIO.setup(STEP, GPIO.OUT)

P = GPIO.PWM(STEP,feq)
p.start(0)

while True
sleep(1)

GPIO.output(DIR, GPIO.HIGH)
p.ChangeDuty Cycle(DUTY_F)
```

Appendix B: Matlab Algorithm for Thickness Determination

B.1 Main Program

```
clear;
clc;
close all;
global I M N step
%% loading image and initialization
I =  imread('006-010.jpg');
step = 1;
[M,N,~] = size(I);
cen_min = 0.3*M; %seperate the part contains the rotational center
cen_max = 0.8*M;
%% Processing
[I_center,I_contour,I_scale_um] = Im_sep(cen_min,cen_max); %seperate image
I_contour = flip(I_contour ,2);    %horizontoal filp for the better contour
shape.
[scalar_I_um,scal_location] = scalar_um(I_scale_um); %convert unit from
pixels to um (um/pi)
[centers,radii,bw_cen] = center_find(I_center); %find the center of the
sample
[C_dist,C_thick,xin,xout,yin,yout] = linear_calc(I_contour,centers);%Find the
inner and outer contour with a linear scan
[ver] = linear_reg(xin,yin);%find out the slope of the line that is
perpendicular to the inner contour
[xver,yver] = ver_dec(xin,yin,centers,ver,I_contour);%Determine the outer
contour with the perpendicular line correspond to each of the point on inner
contour
c_r = centers(1,1);%Pull out the value of the rotation center
c_c = centers(1,2);
%%
thick_con = zeros(1,1); %initialize the thickness and calculate it's value
for z = 1:length(xin)
    dis_in (z) = sqrt((xin(z)-c_c)^2+(yin(z)-c_r)^2); %distance form center to inner contour
    dis_out (z) = sqrt((xout(z)-c_c)^2+(yout(z)-c_r)^2); %distance form
center to outer contour
    dis_ver(z) = sqrt((xver(z)-c_c)^2+(yver(z)-c_r)^2);  %distance form
center to outer contour found by arc approach
    thick_con (z) = sqrt((xver(z)-xin(z))^2+(yver(z)-yin(z))^2); %thichness
calculation base on the inner contour and arc approach
end

%% Ploting
ang =0:359;
```

```matlab
figure(1); %ploting the rotational center on the original figure
imshow(I_center);
hold on
plot(centers(:,1),centers(:,2),'b*')
viscircles(centers,radii);
hold off
title('center found');
figure(2); %ploting the points of inner contour and outer contour that
calculated with two method on the original figure
imshow(I_contour);
hold on
plot (xin, yin,'b');
plot (xout,yout,'r');
plot (xver,yver,'g-');
hold off;
axis equal
title('Contour found overlaped with original image');
figure(3); %ploting the points of inner contour and outer contour that
calculated with two method
hold on
plot (xin, yin,'b');
plot (xout,yout,'r');
plot (xver,yver,'g');
hold off;
axis equal
figure(4); %ploting the distance from the rotational center to the inner and
outer contour
plot(ang,dis_in,'b')
hold on
plot(ang,dis_out,'r')
plot(ang,dis_ver,'g')
figure(5) %ploting the deposit thickness
plot(ang,thick_con,'b')
```

B.2 Image Separation Function

```matlab
function [center,contour,scale_im] = Im_sep(min,max)
global I M N

center = zeros(M,N,3);
contour = zeros(M,N,3);
scale_im = zeros(M,N,3);
scale_range = 500;

for c = 1:N
    for r = 1:M
        if (r>min)&&(r<max)&&(c>min)&&(c<max)
            center(r,c,1) = I(r,c,1);
            contour(r,c,1) = 0;

            center(r,c,2) = I(r,c,2);
```

77

```matlab
            contour(r,c,2) = 0;

            center(r,c,3) = I(r,c,3);
            contour(r,c,3) = 0;

        else
            center(r,c,1) = 0;
            contour(r,c,1) = I(r,c,1);
            center(r,c,2) = 0;
            contour(r,c,2) = I(r,c,2);

            center(r,c,3) = 0;
            contour(r,c,3) = I(r,c,3);

        end
        if (r>M-scale_range)&&(c>M-scale_range)
            if I(r,c,1) >= 253 && I(r,c,2) >= 253 && I(r,c,3) >= 253
                scale_im(r,c,1) = 255;
                scale_im(r,c,2) = 255;
                scale_im(r,c,3) = 255;
                center(r,c,1) = 0;
                contour(r,c,1) = 0;
                center(r,c,2) = 0;
                contour(r,c,2) = 0;
                center(r,c,3) = 0;
                contour(r,c,3) = 0;
            else
                scale_im(r,c) = 0;
            end
        end

    end
end

center = uint8(center);
contour = uint8(contour);
scale_im = uint8(scale_im);
for c = 1:N
    for r = 1:M
        if contour(r,c,1) >= 20 && contour(r,c,2) >= 20 && contour(r,c,3) >=
20
            contour(r,c,1) = 255;
            contour(r,c,2) = 255;
            contour(r,c,3) = 255;
        else
            contour(r,c,1) = 0;
            contour(r,c,2) = 0;
            contour(r,c,3) = 0;
        end
    end
end
contour = im2bw(contour,0.5);
end
```

B.3 Scale Reading Function

```matlab
function [scalar_I_um,scal_location] = scalar_um(I_scale_um)

global M N
bw_scal = imbinarize(I_scale_um);
scal_location = zeros(1,3);
cont = 1;

for r = 1:M
    for c = 1:N
        if bw_scal(r,c) ~= 0
            scal_location(1,cont) = c;
            cont = cont + 1;
        end
    end
end

if cont>111
    fprintf('Maybe noise on the scale plot')
end

scalar_max = max(scal_location);
scalar_min = min(scal_location(scal_location>0));

scalar_I_um = 1000/(scalar_max - scalar_min);
end
```

B.4 Rotation Center Find Function

```matlab
function [centers,radii,bw_cen] = center_find(I_center)
global M N
Center_im = I_center;
for r = 1:M
    for c = 1:N
        if Center_im(r,c,1)>30 || Center_im(r,c,2)>30 || Center_im(r,c,3)>30
            Center_im(r,c,1) = 255;
            Center_im(r,c,2) = 255;
            Center_im(r,c,3) = 255;
        end
    end
end

bw_cen = im2bw(Center_im,0.5);
%% Filting the circle
bw_cen = bwareaopen(bw_cen,50); %close pixels area smaller than 50
bw_cen = imfill(bw_cen,'holes'); %fill all holes
%% Find the center
```

79

```matlab
Icir = bw_cen;
dim = size(Icir);
col = round(dim(2)/2)-90;
row = min(find(Icir(:,col)));
boundary = bwtraceboundary(Icir,[row, col],'N');
boundaries = bwboundaries(Icir);
b = boundaries{1};
s = regionprops('table',Icir,'Centroid',...
    'MajorAxisLength','MinorAxisLength');
centers = cat(1,s.Centroid);
diameters = mean([s.MajorAxisLength s.MinorAxisLength],2);
radii = diameters/2;
end
```

B.5 Inner and Outer Contour Linear Scan Function

```matlab
function [C_dist,C_thick,xin,xout,yin,yout] = linear_calc(I_contour,centers)
global M N
%% fix center to integer
c_r = centers(:,1);
c_c = centers(:,2);
%% Loop
row_cont = 0;
for theta = 0:1:359

    row_cont = row_cont+1;
    col_cont = 1;
    rad_conv = pi/180; % initialize cont and angle in radius

    if (theta==0)
        for r = c_r:-1:1
            if I_contour(r,c_c) == 1
                Con_r(row_cont,col_cont) = r;
                Con_c(row_cont,col_cont) = c_c;
                col_cont = col_cont+1;
            end
        end
        xin(1,row_cont) = c_c;
        xout(1,row_cont) = c_c;
        yin(1,row_cont) = Con_r(row_cont,1);
        row_y = Con_r(row_cont,:);
        yout(1,row_cont) = min(row_y(row_y>0));

    elseif (theta<=45)
        for r = 1:c_r-1
            c = r*tan(theta*rad_conv);
            c = round(c);
            if c < N-c_c
                if I_contour(c_r-r,c_c+c) == 1
                    Con_r(row_cont,col_cont) = c_r-r;
                    Con_c(row_cont,col_cont) = c_c+c;
                    col_cont = col_cont+1;
```

```matlab
                end
            end
        end
        xin(1,row_cont) = Con_c(row_cont,1);
        row_x = Con_c(row_cont,:);
        xout(1,row_cont) = max(row_x);
        yin(1,row_cont) = Con_r(row_cont,1);
        row_y = Con_r(row_cont,:);
        yout(1,row_cont) = min(row_y(row_y>0));
    elseif (theta<90)
        for c = 1:N-c_c-1
            r = tan((90-theta)*rad_conv)*c;
            r = round(r);
            if r < c_r-1
                if I_contour(c_r-r,c_c+c) == 1
                    Con_r(row_cont,col_cont) = c_r-r;
                    Con_c(row_cont,col_cont) = c_c+c;
                    col_cont = col_cont+1;
                end
            end
        end
        xin(1,row_cont) = Con_c(row_cont,1);
        row_x = Con_c(row_cont,:);
        xout(1,row_cont) = max(row_x);
        yin(1,row_cont) = Con_r(row_cont,1);
        row_y = Con_r(row_cont,:);
        yout(1,row_cont) = min(row_y(row_y>0));


    elseif (theta==90)
        for c = c_c:N-1
            if I_contour(c_r,c) == 1
                Con_r(row_cont,col_cont) = c_r;
                Con_c(row_cont,col_cont) = c;
                col_cont = col_cont+1;
            end
        end

        xin(1,row_cont) = Con_c(row_cont,1);
        row_x = Con_c(row_cont,:);
        xout(1,row_cont) = max(row_x);
        yin(1,row_cont) = c_r;
        yout(1,row_cont) = c_r;

    elseif (theta<135)
        for c = 1:N-c_c-1
            r = c*tan((theta-90)*rad_conv);
            r = round(r);
            if r < M-c_r
                if I_contour(c_r+r,c_c+c) == 1
                    Con_r(row_cont,col_cont) = c_r+r;
                    Con_c(row_cont,col_cont) = c_c+c;
                    col_cont = col_cont+1;
                end
            end
```

81

```matlab
        end
    xin(1,row_cont) = Con_c(row_cont,1);
    row_x = Con_c(row_cont,:);
    xout(1,row_cont) = max(row_x);
    yin(1,row_cont) = Con_r(row_cont,1);
    row_y = Con_r(row_cont,:);
    yout(1,row_cont) = max(row_y);

elseif (theta<180)
    for r = 1:M-c_r-1
        c = r*tan((180-theta)*rad_conv);
        c = round(c);
        if c < N-c_c
            if I_contour(c_r+r,c_c+c) == 1
                Con_r(row_cont,col_cont) = c_r+r;
                Con_c(row_cont,col_cont) = c_c+c;
                col_cont = col_cont+1;
            end
        end
    end
    xin(1,row_cont) = Con_c(row_cont,1);
    row_x = Con_c(row_cont,:);
    xout(1,row_cont) = max(row_x);
    yin(1,row_cont) = Con_r(row_cont,1);
    row_y = Con_r(row_cont,:);
    yout(1,row_cont) = max(row_y);

elseif (theta==180)
    for r = c_r:M-1
        if I_contour(r,c_c) == 1
            Con_r(row_cont,col_cont) = r;
            Con_c(row_cont,col_cont) = c_c;
            col_cont = col_cont+1;
        end
    end
    xin(1,row_cont) = c_c;
    xout(1,row_cont) = c_c;
    yin(1,row_cont) = Con_r(row_cont,1);
    row_y = Con_r(row_cont,:);
    yout(1,row_cont) = max(row_y);

elseif  (theta <= 225)
    for r = 1:M-c_r-1
        c = r*tan((theta-180)*rad_conv);
        c = round(c);
        if c < c_c
            if I_contour(c_r+r,c_c-c) == 1
                Con_r(row_cont,col_cont) = c_r+r;
                Con_c(row_cont,col_cont) = c_c-c;
                col_cont = col_cont+1;
            end
        end
    end

    xin(1,row_cont) = Con_c(row_cont,1);
```

```matlab
        row_x = Con_c(row_cont,:);
        xout(1,row_cont) = min(row_x(row_x>0));
        yin(1,row_cont) = Con_r(row_cont,1);
        row_y = Con_r(row_cont,:);
        yout(1,row_cont) = max(row_y);

    elseif (theta<270)
        for c = 1:c_c-1
            r = c*tan((270-theta)*rad_conv);
            r = round(r);
            if r < M-c_r
                if I_contour(c_r+r,c_c-c) == 1
                    Con_r(row_cont,col_cont) = c_r+r;
                    Con_c(row_cont,col_cont) = c_c-c;
                    col_cont = col_cont+1;
                end
            end
        end

        xin(1,row_cont) = Con_c(row_cont,1);
        row_x = Con_c(row_cont,:);
        xout(1,row_cont) = min(row_x(row_x>0));
        yin(1,row_cont) = Con_r(row_cont,1);
        row_y = Con_r(row_cont,:);
        yout(1,row_cont) = max(row_y);

    elseif (theta==270)
        for c = c_c:-1:1
            if I_contour(c_r,c) == 1
                Con_r(row_cont,col_cont) = c_r;
                Con_c(row_cont,col_cont) = c;
                col_cont = col_cont+1;
            end
        end
        xin(1,row_cont) = Con_c(row_cont,1);
        row_x = Con_c(row_cont,:);
        xout(1,row_cont) = min(row_x(row_x>0));
        yin(1,row_cont) = c_r;
        yout(1,row_cont) = c_r;

    elseif (theta < 315)
        for c = 1:c_c-1
            r = tan((theta-270)*rad_conv);
            r = round(r);
            if r < c_r
                if I_contour(c_r-r,c_c-c) == 1
                    Con_r(row_cont,col_cont) = c_r-r;
                    Con_c(row_cont,col_cont) = c_c-c;
                    col_cont = col_cont+1;
                end
            end
        end
        xin(1,row_cont) = Con_c(row_cont,1);
        row_x = Con_c(row_cont,:);
        xout(1,row_cont) = min(row_x(row_x>0));
```

```matlab
        yin(1,row_cont) = Con_r(row_cont,1);
        row_y = Con_r(row_cont,:);
        yout(1,row_cont) = min(row_y(row_y>0));

    else
        for r = 1:c_r-1
            c = r*tan((360-theta)*rad_conv);
            c = round(c);
            if c < c_c
                if I_contour(c_r-r,c_c-c) == 1
                    Con_r(row_cont,col_cont) = c_r-r;
                    Con_c(row_cont,col_cont) = c_c-c;
                    col_cont = col_cont+1;
                end
            end
        end

        xin(1,row_cont) = Con_c(row_cont,1);
        row_x = Con_c(row_cont,:);
        xout(1,row_cont) = min(row_x(row_x>0));
        yin(1,row_cont) = Con_r(row_cont,1);
        row_y = Con_r(row_cont,:);
        yout(1,row_cont) = min(row_y(row_y>0));
    end

end
```

B.6 Inner Contour Perpendicular Line Finding Function

```matlab
function [ver] = linear_reg(xin,yin)
%%
len = length(xin);
slope = zeros(1,3);
ver = zeros(1,3);
    for i = 1:len
        if i == 1
            x = [xin(len) xin(1) xin(2)];
            y = [yin(len) yin(1) yin(2)];
            p = polyfit(x,y,2);
            a = p(1);
            b = p(2);
            slope(i) = 2*a*xin(1)+b;
            ver(i) = -1/slope(i);
        elseif i == len
            x = [xin(len-1) xin(len) xin(1)];
            y = [yin(len-1) yin(len) yin(1)];
            p = polyfit(x,y,2);
            a = p(1);
            b = p(2);
            slope(i) = 2*a*xin(len)+b;
            ver(i) = -1/slope(i);
```

84

```
        else
            x = [xin(i-1) xin(i) xin(i+1)];
            y = [yin(i-1) yin(i) yin(i+1)];
            p = polyfit(x,y,2);
            a = p(1);
            b = p(2);
            slope(i) = 2*a*xin(i)+b;
            ver(i) = -1/slope(i);
        end
    end
end
```

B.7 Points on the Contour Corresponding to the Thickness Function

```
function [xver,yver] = ver_dec(xin,yin,centers,ver,I_contour)
global M N
contour_len = length(xin);
b_offset = zeros(1,3);
c_r = centers(1,1);
c_c = centers(1,2);
c_r = round(c_r);
c_c = round(c_c);
dis = zeros(1,1);
y = zeros(1,1);
x = zeros(1,1);
xver = zeros(1,1);
yver = zeros(1,1);
tol = 50;
row_cont = 0;
Ver_x = zeros(1,3);
Ver_y = zeros(1,3);
row_x = zeros(1,46);
row_y = zeros(1,46);
%%
for i = 1:360
    row_cont = row_cont+1;
    col_cont = 1;
    b_offset(1,i) = yin(1,i)-ver(1,i)*xin(1,i);

    if i < 45
        for y =c_r-1:-0.001:1
            x = (y-b_offset(i))/ver(i);
            x = round(x);
            y = round(y);
            if x < N && x > c_c-tol && y <850
                if I_contour(y,x)==1
                    Ver_x(row_cont,col_cont) = x;
                    Ver_y(row_cont,col_cont) = y;
                    col_cont = col_cont+1;
                end
            end
```

```
        end
    row_x = Ver_x(row_cont,:);
    xver(1,row_cont) = max(row_x);
    row_y = Ver_y(row_cont,:);
    yver(1,row_cont) = min(row_y(row_y>0));

elseif i < 90
    for x = c_c:0.01:N-1
        y = ver(i)*x + b_offset(i);
        x = round(x);
        y = round(y);
        if y < c_r &&y>0
            if I_contour(y,x)==1
                Ver_x(row_cont,col_cont) = x;
                Ver_y(row_cont,col_cont) = y;
                col_cont = col_cont+1;
            end
        end
    end
    row_x = Ver_x(row_cont,:);
    xver(1,row_cont) = max(row_x);
    row_y = Ver_y(row_cont,:);
    yver(1,row_cont) = min(row_y(row_y>0));

    elseif i < 135
    for x = c_c:0.01:N-1
        y = ver(i)*x + b_offset(i);
        x = round(x);
        y = round(y);
        if y > c_r-tol && y < M
            if I_contour(y,x)==1
                Ver_x(row_cont,col_cont) = x;
                Ver_y(row_cont,col_cont) = y;
                col_cont = col_cont+1;
            end
        end
    end
    row_x = Ver_x(row_cont,:);
    xver(1,row_cont) = max(row_x);
    row_y = Ver_y(row_cont,:);
    yver(1,row_cont) = max(row_y);

    elseif i < 180
    for y = c_r:0.01:M-1
        x = (y-b_offset(i))/ver(i);
        x = round(x);
        y = round(y);
        if x > c_c-tol && x < N
            if I_contour(y,x)==1
                Ver_x(row_cont,col_cont) = x;
                Ver_y(row_cont,col_cont) = y;
                col_cont = col_cont+1;
            end
        end
    end
    end
```

```matlab
row_x = Ver_x(row_cont,:);
xver(1,row_cont) = max(row_x);
row_y = Ver_y(row_cont,:);
yver(1,row_cont) = max(row_y);

elseif i < 225
  for y = M-1:-0.001:c_r
      x = (y-b_offset(i))/ver(i);
      x = round(x);
      y = round(y);
       if x < c_c+tol && x >0
           if I_contour(y,x)== 1
               Ver_x(row_cont,col_cont) = x;
               Ver_y(row_cont,col_cont) = y;
               col_cont = col_cont+1;
           end
       end
  end
row_x = Ver_x(row_cont,:);
xver(1,row_cont) = min(row_x(row_x>0));
row_y = Ver_y(row_cont,:);
yver(1,row_cont) = max(row_y);

elseif i < 270
  for x = 1:0.01:c_c
      y = ver(i)*x + b_offset(i);
      x = round(x);
      y = round(y);
       if y > c_r-tol && y < M
           if I_contour(y,x)==1
               Ver_x(row_cont,col_cont) = x;
               Ver_y(row_cont,col_cont) = y;
               col_cont = col_cont+1;
           end
       end
  end
row_x = Ver_x(row_cont,:);
xver(1,row_cont) = min(row_x(row_x>0));
row_y = Ver_y(row_cont,:);
yver(1,row_cont) = max(row_y);

elseif i < 315
  for x = 1:0.01:c_c
      y = ver(i)*x + b_offset(i);
      x = round(x);
      y = round(y);
       if y < c_r+tol&&x>0
           if I_contour(y,x)==1
               Ver_x(row_cont,col_cont) = x;
               Ver_y(row_cont,col_cont) = y;
               col_cont = col_cont+1;
           end
       end
  end
row_x = Ver_x(row_cont,:);
```

```matlab
            xver(1,row_cont) = min(row_x(row_x>0));
            row_y = Ver_y(row_cont,:);
            yver(1,row_cont) = min(row_y(row_y>0));

        else
            for y = 1:0.01:c_r
                x = (y-b_offset(i))/ver(i);
                x = round(x);
                y = round(y);
                 if x < c_c+1500 && x > 0
                    if I_contour(y,x)==1
                        Ver_x(row_cont,col_cont) = x;
                        Ver_y(row_cont,col_cont) = y;
                        col_cont = col_cont+1;
                    end
                end
            end
        row_x = Ver_x(row_cont,:);
        xver(1,row_cont) = min(row_x(row_x>0));
        row_y = Ver_y(row_cont,:);
        yver(1,row_cont) = min(row_y(row_y>0));
    end
end
end
```

Appendix C: Matlab Algorithm for Mandrel Correction

C.1 Main Program

```matlab
clear;
clc;
close all;

%% loading image and initialization
theta = 0:359;
for i = 1:length(theta)
    th = theta(i)*pi/180;
    r(i) = 0.7*(2-0.15*sin(6*th)+0.2*cos(12*th));
    xin(i) = r(i)*cos(th);
    yin(i) = r(i)*sin(th);
end
thickness = 0.11;
k = 0.05;
centers = [0,0];
R_0 = 1.5;
Ei = k*(r-R_0);
[alpha] = alpha_calc(xin,yin);

delta = Ei./cos(deg2rad(alpha));

P_c = r+abs(delta);

inc=2*pi/360;
theta = inc:inc:2*pi;
polarplot(theta,r,'b');
hold on
polarplot(theta,P_c,'r');
```

C.2 Angle Alpha Calculation Function

```matlab
function [alpha] = alpha_calc(xin,yin)

len = length(xin);
slope = zeros(1,3);
ver = zeros(1,3);
offset = zeros(1,3);
```

```matlab
    for i = 1:len
        if i == 1
            x = [xin(len) xin(1) xin(2)];
            y = [yin(len) yin(1) yin(2)];
            p = polyfit(x,y,2);
            a = p(1);
            b = p(2);
            slope(i) = 2*a*xin(1)+b;
            ver(i) = -1/slope(i);
            alpha(i) = rad2deg(atan(ver(i)))-(i-1);
        elseif i == len
            x = [xin(len-1) xin(len) xin(1)];
            y = [yin(len-1) yin(len) yin(1)];
            p = polyfit(x,y,2);
            a = p(1);
            b = p(2);
            slope(i) = 2*a*xin(len)+b;
            ver(i) = -1/slope(i);
            alpha(i) = rad2deg(atan(ver(i)))-(i-1);
        else
            x = [xin(i-1) xin(i) xin(i+1)];
            y = [yin(i-1) yin(i) yin(i+1)];
            p = polyfit(x,y,2);
            a = p(1);
            b = p(2);
            slope(i) = 2*a*xin(i)+b;
            ver(i) = -1/slope(i);
            alpha(i) = rad2deg(atan(ver(i)))-(i-1);
        end
    end
end
```